

Influence of Synoptic Sea-Breeze Fronts on the Urban Heat Island Intensity in Dallas–Fort Worth, Texas

XIAO-MING HU AND MING XUE

*Center for Analysis and Prediction of Storms, and School of Meteorology,
University of Oklahoma, Norman, Oklahoma*

(Manuscript received 22 May 2015, in final form 28 September 2015)

ABSTRACT

When assessed using the difference between urban and rural air temperatures, the urban heat island (UHI) is most prominent during the nighttime. Typically, nocturnal UHI intensity is maintained throughout the night. The UHI intensity over Dallas–Fort Worth (DFW), Texas, however, experienced frequent “collapses” (sudden decreases) around midnight during August 2011, while the region was experiencing an intense heat wave. Observational and modeling studies were conducted to understand this unique phenomenon. Sea-breeze passage was found to be ultimately responsible for the collapses of the nocturnal UHI. Sea-breeze circulation developed along the coast of the Gulf of Mexico during the daytime. During the nighttime, the sea-breeze circulation was advected inland (as far as ~ 400 km) by the low-level jet-enhanced southerly flow, maintaining the characteristics of sea-breeze fronts, including the enhanced wind shear and vertical mixing. Ahead of the front, surface radiative cooling enhanced the near-surface temperature inversion in rural areas through the night with calm winds. During the frontal passage (around midnight at DFW), the enhanced vertical mixing at the leading edge of the fronts brought warmer air to the surface, leading to rural surface warming events. In contrast, urban effects led to a nearly neutral urban boundary layer. The enhanced mechanical mixing associated with sea-breeze fronts, therefore, did not increase urban surface temperature. The different responses to the sea-breeze frontal passages between rural (warming) and urban areas (no warming) led to the collapse of the UHI. The inland penetration of sea-breeze fronts at such large distances from the coast and their effects on UHI have not been documented in the literature.

1. Introduction

In numerous studies, temperatures over urban areas have been found to be typically higher than over surrounding rural areas. This phenomenon is commonly known as the urban heat island (UHI; Oke 1976, 1981, 1982; Arnfield 2003). Because of rapid urbanization during the past few decades around the world, UHI has been the subject of increasingly more investigations. UHI intensity is normally defined/quantified as the difference between urban and rural near-surface temperatures, typically at 2 m above ground. UHI intensity in such a traditionally defined quantity can be easily measured (e.g., Basara et al. 2008) and can be reproduced by model simulations reasonably well (e.g., Hu et al. 2013c).

Through many observational and modeling studies, understanding of this urban effect is improved during the past few decades. UHI shows a prominent diurnal cycle with lower intensity (even negative at times) during daytime and higher intensity at night primarily due to nighttime release of the heat stored in the building materials during the day (Chen et al. 2014), thus UHI is primarily a nocturnal phenomenon (Tumanov et al. 1999; Arnfield 2003; Souch and Grimmond 2006; Basara et al. 2008; Lemonsu et al. 2009; Memon et al. 2009; Camilloni and Barrucand 2012; Cui and de Foy 2012; Hu et al. 2013c; Theeuwes et al. 2013; Dou et al. 2015). UHI intensity normally increases around sunset quickly and then stays at a roughly constant level throughout the night until early next morning when the convective boundary layer develops rapidly. Such UHI characteristics have been documented for a number of major cities, such as Bucharest, Romania (Tumanov et al. 1999); Paris, France (Lemonsu and Masson 2002); Phoenix, Arizona (Fast et al. 2005); London, United Kingdom (Bohenstengel et al. 2011); Thessaloniki and Athens, Greece (Giannaros

Corresponding author address: Dr. Xiao-Ming Hu, Center for Analysis and Prediction of Storms, and School of Meteorology, University of Oklahoma, 120 David L. Boren Blvd., Norman, OK 73072.
E-mail: xhu@ou.edu

and Melas 2012; Giannaros et al. 2013); Beijing, China (Yang et al. 2013); and Oklahoma City, Oklahoma (Basara et al. 2008; Hu et al. 2013c). Certain detailed temporal variations (e.g., at hourly time scales) of nighttime UHI intensity, however, remain unexplained (Hu et al. 2013c). A few meteorological factors (e.g., cloudiness and wind speed) were found to affect UHI intensity (Fast et al. 2005; Souch and Grimmond 2006; Lee et al. 2012; Smoliak et al. 2015). Investigation of UHI of Oklahoma City further demonstrated that the structure of nocturnal boundary layer plays an important role in modulating UHI intensity (Hu et al. 2013c).

The cities of Dallas ($32^{\circ}46'N$, $96^{\circ}48'W$) and Fort Worth, Texas ($32^{\circ}45'N$, $97^{\circ}19'W$), are located in north-central Texas, in the upper margin of the coastal plain, approximately 400 km northwest of the Gulf of Mexico (Fig. 1). During the past few decades, due to rapid industrialization and urbanization, the two cities now form a single “Metroplex.” The Dallas–Fort Worth (DFW) area is now the fourth-largest metropolitan area in the United States. Significant urbanization around the DFW area resulted in prominent UHIs. UHI intensity, quantified as the difference in temperature at 2 m between urban and rural areas, reached 5.4°C in July 2011 (Winguth and Kelp 2013). The widespread UHI around the DFW area plays an important role in influencing regional climate (Winguth and Kelp 2013). Further urbanization is anticipated around the DFW area. By 2050, the DFW area is projected to be a “megacity” with ~ 15 million inhabitants and the UHI in future scenarios is projected to be more severe (Li and Bou-Zeid 2013; Winguth and Kelp 2013). Thus, UHI is projected to play more important roles in the future in modulating boundary layer meteorology, air quality, and climate of the DFW region.

A severe heat wave struck the region around DFW in the summer of 2011. Frequency of similar heat waves is likely to increase over most land areas in the twenty-first century according to the Intergovernmental Panel on Climate Change (IPCC 2007). Of all documented weather hazards, heat waves cause the most fatalities annually within the United States (Changnon et al. 1996; Davis et al. 2003). UHI plays a critical role in further exacerbating the detrimental environmental conditions during heat wave events (Basara et al. 2010; Tan et al. 2010; Chen et al. 2014), thus having a major impact on large urban populations. Investigation and understanding of the UHIs during heat waves, however, is limited by a lack of high-quality surface observations with long-term consistency; such data are vital for study of the UHIs (Basara et al. 2010). In this study, we aim to investigate rapid temporal variations and their causes in nocturnal UHI intensity of DFW in the summer of 2011, using a long-term, consistent, and research-quality dataset as well as three-dimensional model simulations.

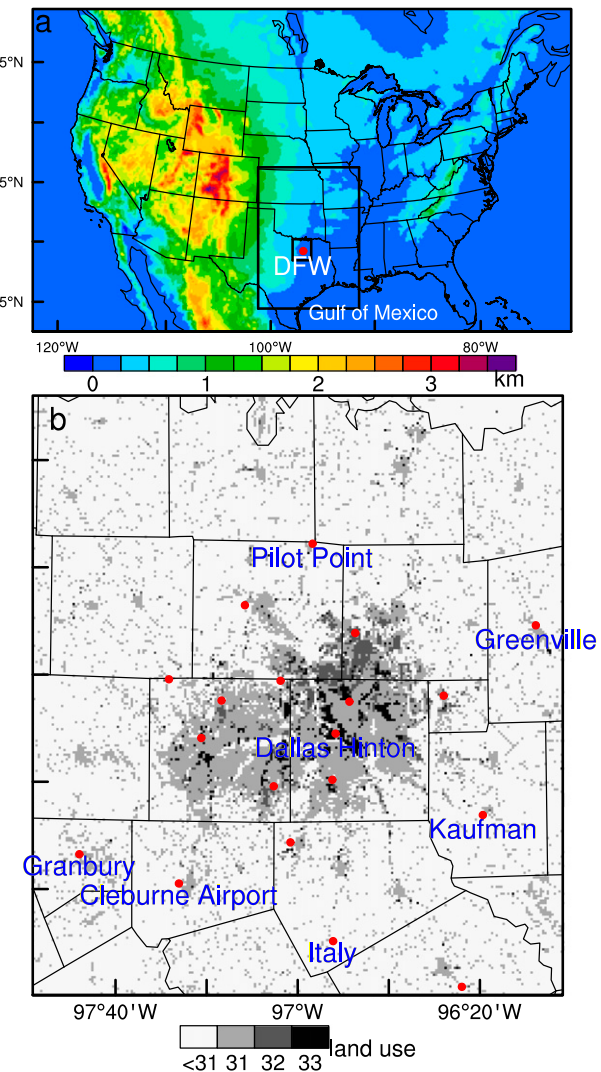


FIG. 1. (a) Map of model domains and terrain height and (b) urban land-use categories (i.e., 31, 32, and 33) in domain 3. The locations of TCEQ CAMS sites around DFW are marked in (b).

Because of the thermal contrast between the warm land and cool sea during the day, a local circulation, called sea breeze, occurs frequently along the Gulf of Mexico under suitable conditions (Hsu 1970, 1988; Banta et al. 2005). After sunset, radiative cooling prevails, the land-sea thermal difference reverses, and a mirror process, called land breeze, develops in the presence of the Coriolis force (Yan and Anthes 1987; Miller et al. 2003; Qian et al. 2012). Depending on the direction of the prevailing wind (PW), sea breeze can be classified into four categories: pure, corkscrew, backdoor, and synoptic (Miller et al. 2003). A synoptic sea breeze occurs when the PW is onshore, while the other three categories (i.e., pure, corkscrew, and backdoor) occur when the PW has an offshore component. The three categories with offshore

wind components are further differentiated by their different alongshore wind components: pure (with zero alongshore component), corkscrew (with alongshore component with land to the left), and backdoor (with alongshore component with land to the right) (Miller et al. 2003). Previous studies mostly focused on the pure, corkscrew, and backdoor sea breezes while the studies for the synoptic sea breeze were fewer (Miller et al. 2003; Porson et al. 2007; Crosman and Horel 2010; Steele et al. 2013, 2015), likely because the onshore PW normally suppresses the synoptic sea-breeze circulation (Helmis et al. 1987; Arritt 1993; Finkle et al. 1995). Also most previous studies have focused on the development and maintenance of the sea breeze during daylight hours, but have not extensively investigated its subsequent nocturnal evolution. Investigation of the nocturnal sea breeze is limited because good boundary layer observational data are lacking, and previous studies may have considered such events rare and less important (Garratt and Physick 1985; Buckley and Kurzeja 1997; Tijm et al. 1999; Abatan et al. 2014).

Some studies had been conducted to investigate the relationship between the urban effects and sea breeze. Most of them focused on the influence of urban effects on the dynamics of sea breeze (e.g., Sarkar et al. 1998; Ohashi and Kida 2002; Childs and Raman 2005; Freitas et al. 2007; Thompson et al. 2007; Cheng and Byun 2008; Dandou et al. 2009; Keeler and Kristovich 2012; Li et al. 2015). It remains unclear to what extent sea-breeze dynamics affect the UHI development and intensity. The temporal variation of UHI of DFW (focusing on nighttime) and its response to sea-breeze frontal passages are investigated in this study.

The rest of this paper is organized as follows: in section 2, episode selection, datasets, and configurations of the Weather Research and Forecasting (WRF) Model simulations used in this study are described. In section 3, sea-breeze development and its impact on nocturnal UHIs of DFW are examined using observations and model simulations. The paper concludes in section 4 with a summary of the main findings and a discussion about the implications for air quality.

2. Data and methods

a. Episodes and observations

During July and August of 2011, an intense heat wave impacted the southern Great Plains, including Oklahoma and Texas (Winguth and Kelp 2013; Ramsey et al. 2014; Tadesse et al. 2015), which was likely related to the cold sea surface temperature anomalies in the tropical Pacific Ocean (i.e., a La Niña condition) and a positive phase of the Atlantic multidecadal oscillation (Nielsen-Gammon

2012). Since the UHI of DFW in July 2011 was discussed in Winguth and Kelp (2013), this study will focus on the month of August 2011, with a particular attention to the night of 7–8 August. A long-term, consistent, and research-quality dataset [same as used in Winguth and Kelp (2013)] is used in this study for the analysis of UHIs in DFW [i.e., hourly data collected from the Continual Ambient Monitoring Stations (CAMS) implemented by the Texas Commission for Environmental Quality (TCEQ) and archived by the U.S. Environmental Protection Agency; EPA (2015)]. The UHI intensity is quantified using two approaches: first as the temperature difference between the representative urban (Dallas Hinton, CAMS 60) and rural (Kaufman, CAMS 71) stations following the same approach as Winguth and Kelp (2013) [see Winguth and Kelp (2013) for detailed rationales for the site selection], and second as the temperature difference between Dallas Hinton and the surrounding six rural sites (see their locations in Fig. 1b) to avoid possible temperature bias at certain individual rural sites following the approach of Hu et al. (2013c).

The regional-scale meteorological conditions are examined using the surface mesonet data archived by the Meteorological Assimilation Data Ingest System (MADIS) developed by National Oceanic and Atmospheric Administration (NOAA). Because MADIS mesonet integrated data from many providers, small-scale spatial heterogeneity would be an issue when examining the regional meteorological condition. To alleviate this issue, instead of spatial distribution of instantaneous meteorological variables, meteorological tendency (i.e., difference between the current and next hours) is computed to examine temporal variations of meteorological conditions. In the spatial distribution of meteorological tendency, the small-scale local heterogeneity in instantaneous values is removed and only the spatial information of temporal variation (modulated by larger-scale external forcing) remains. As will be shown later, the external forcing associated with sea-breeze frontal movement can be clearly identified in the spatial distribution of observed meteorological tendencies and it played an important role in modulating the nocturnal UHI intensities of DFW.

Other datasets used to illustrate the development of the sea breeze and its impacts include the High Vertical Resolution Radiosonde Data (HVRRD), the nighttime land surface temperatures retrieved from Moderate Resolution Imaging Spectroradiometer (MODIS) data, and air quality data at the TCEQ CAMS sites.

b. Three-dimensional simulations

To investigate the development of sea breezes and their impacts on the UHIs around DFW, three-dimensional simulations with the WRF Model (Skamarock et al. 2008),

version 3.6.1, were conducted for 7–8 August 2011. Following the approach of Hu et al. (2013c), the simulation was initialized at 0000 UTC [UTC = central standard time (CST) + 6 h] on 7 August 2011 to allow enough spinup for the UHI to develop on the night of 7–8 August. Three one-way nested domains (Fig. 1) were employed with horizontal grid spacings of 12, 4, and 0.8 km, respectively. Each domain had 48 vertical layers extending from the surface to 100 hPa. The lowest 20 model sigma levels are at 1.0, 0.997, 0.994, 0.991, 0.988, 0.985, 0.975, 0.97, 0.96, 0.95, 0.94, 0.93, 0.92, 0.91, 0.895, 0.88, 0.865, 0.85, 0.825, and 0.8 (the corresponding midlevel heights of each model layer are about 12, 37, 61, 86, 111, 144, 186, 227, 290, 374, 459, 545, 631, 717, 826, 958, 1092, 1226, and 1409 m above ground). Such horizontal and vertical resolutions were shown to be adequate to capture boundary layer structures and UHI characteristics (Liu et al. 2006; Hu et al. 2013c). All model domains used the Yonsei University (YSU) PBL scheme (Hong et al. 2006; Hu et al. 2013a), the Dudhia shortwave radiation algorithm (Dudhia 1989), the Rapid Radiative Transfer Model (RRTM; Mlawer et al. 1997) for longwave radiation, and the WRF single-moment 6-class (WSM6) microphysics scheme (Hong et al. 2004). Sensitivity simulations with three other widely used PBL schemes—the Mellor–Yamada–Janjić (Janjić 1990), asymmetric convective model version 2 (ACM2; Pleim 2007a,b), and Bougeault–Lacarrére (Bougeault and Lacarrere 1989) schemes—have also been conducted. These simulations produced similar behaviors as the simulation with the YSU PBL scheme in terms of the development and propagation of the sea-breeze front and their impact on the UHI intensity in Dallas. Thus, only the results from the simulation with the YSU scheme is shown in this paper.

To simulate the thermodynamic and dynamic effects of urban areas on the atmosphere, the Noah land surface scheme (Chen and Dudhia 2001) coupled with a single-layer urban canopy model (SLUCM; Kusaka et al. 2001) was chosen, through which the land surface processes over urban areas are treated by the SLUCM while those over other land-use categories are handled by the Noah scheme. This approach was applied widely to assess the impact of urbanization on our living environments and risks (e.g., Miao et al. 2009; Flagg and Taylor 2011; Salamanca et al. 2011; Hu et al. 2013c; Kim et al. 2013; Li et al. 2013). The urban land-use categories (Fig. 1b) were derived from the 2006 National Land Cover Data (NLCD), in which the urban land use was divided into three categories: low-intensity residential (31), high-intensity residential (32), and commercial/industrial (33). For other regions than the urban area, the U.S. Geological Survey (USGS) land use and soil category data were used in each domain.

The North American Regional Reanalysis (NARR) with a resolution of approximately $0.3^\circ \times 0.3^\circ$ (32 km) was used for the initial conditions (for the atmosphere, soil, and ocean) and boundary conditions. A sensitivity experiment using the National Centers for Environmental Prediction (NCEP) Final (FNL) analysis as the initial and boundary conditions has also been conducted but the results are not shown here. The simulation gave too weak sea-breeze circulations because the FNL data have excessive soil moisture in the southeast Texas (Hu et al. 2010).

The sea surface temperature (SST) is held constant throughout the simulation. A sensitivity simulation with SST updated every 6 h (not shown in this paper) indicates that whether updating SST or not does not affect the sea-breeze development and propagation since the diurnal variation of SST is quite small.

3. Results

a. Time series analysis: Identification of unique characteristics of UHI and their likely cause

The UHI intensity of DFW showed a distinct diurnal pattern (Fig. 2). It increased prominently during the early evening transition and remained positive until the next morning when the rapidly developing convective boundary layer broke down the near-surface inversion. Urban cool island (i.e., negative UHI intensity), even though weak, occurred during the daytime on most days. The nocturnal UHI intensity varied between 2° and 5°C on individual nights during August 2011. The day-to-day variation of the nocturnal UHIs was discussed in previous studies and was believed to be primarily caused by the day-to-day variation of cloud cover and large-scale wind (Morris et al. 2001; Unger et al. 2001; Fast et al. 2005; Steeneveld et al. 2011; Hu et al. 2013c). Such a day-to-day variation will not be the focus of this study.

As summarized in the introduction, a roughly constant UHI intensity throughout the night was reported for many cities (e.g., Hu et al. 2013c). Differently, a sharp decrease of UHI intensity in the later half of the night occurred at DFW on many nights during August 2011 (e.g., 5–11 August, Fig. 3a). On those nights the UHI intensity in the later half of the night was only half of the magnitudes during the early half of the night (Fig. 3a). Such sharp decreases in nocturnal UHI intensity can be clearly identified both when the UHI intensity is quantified as temperature difference between an urban site and a single rural site and when it is defined as the difference between an urban site and mean of multiple rural sites (Figs. 2a,b). To determine the cause for such a sharp decrease (“collapse”) of the nocturnal UHIs is one of the main objectives of the present study.

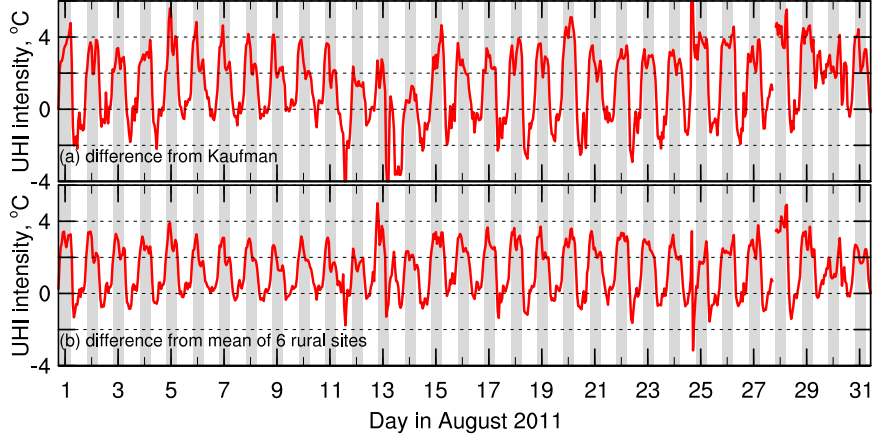


FIG. 2. Time series of observed UHI intensity of DFW quantified as temperature difference (a) between Dallas Hinton and Kaufman and (b) between Dallas Hinton and the mean of six rural sites (i.e., Pilot Point, Greenville, Kaufman, Italy, Cleburne, and Granbury), see the location of these sites in Fig. 1b. Periods of sunset to sunrise are shaded.

The temperature data at representative urban (Dallas Hinton, CAMS 60) and rural (Kaufman, CAMS 71) sites were examined to identify the cause of the collapse. Nocturnal warming events, defined as sudden rise in nighttime surface temperature (White 2009), occurred at the rural site (but not at the urban site) were identified to be primarily responsible (Fig. 3a). Such warming events were reported previously and can be sometimes caused by synoptic-scale cold frontal passages (Doswell and Haugland 2007; Shapiro et al. 2009; Nallapareddy et al. 2011). In such cases, turbulence induced by strong wind shear associated with the cold front mixes warmer air from the upper parts of nighttime stable boundary layer down to the surface, leading to the nocturnal

warming events (Hu et al. 2013b). Examination of surface weather maps suggested that there was no synoptic-scale cold frontal passage around DFW on the nights of 5–11 August (figure not shown). Thus, other reasons rather than synoptic-scale cold frontal passage must be responsible for the nocturnal warming events at the rural site.

Surface wind speeds were examined to investigate the reasons for the rural nocturnal warming events. Surface wind speeds typically peak during the day and decrease during the night due to strong/weak coupling between surface wind and boundary layer momentum during the daytime/nighttime (Hu et al. 2013a; Allen and Washington 2014). However, the diurnal variation of wind speeds

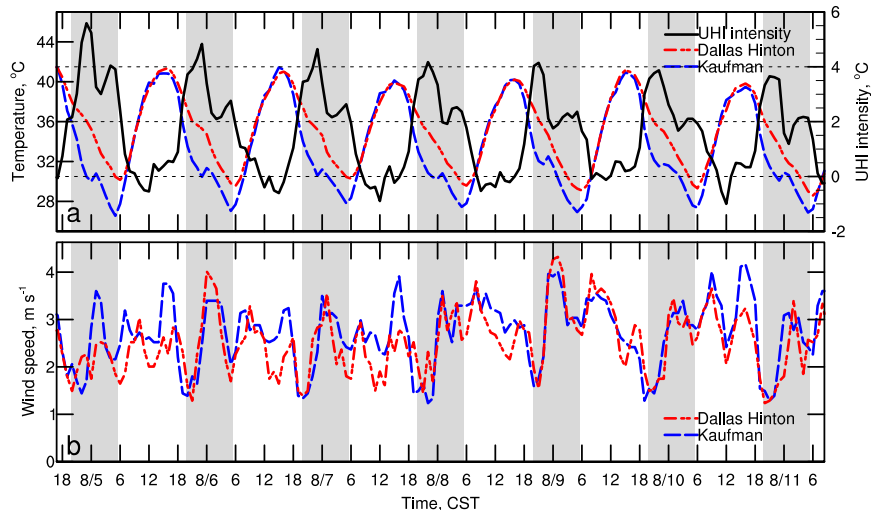


FIG. 3. Time series of observed (a) temperature and UHI intensity and (b) wind speed at Dallas Hinton and Kaufman during 5–11 Aug 2011. Periods of sunset to sunrise are shaded.

around DFW did not follow such a typical pattern. Nocturnal wind maxima occurred around midnight on each night during 5–11 August (Fig. 3b). These nocturnal wind maxima appeared to be highly correlated with the nocturnal warming events at the rural site.

b. Horizontal characteristics of relevant phenomena

WRF simulations were conducted for the period of 5–11 August 2011 to understand the nocturnal wind maximum, warming events, and the collapse of the nocturnal UHIs. Similar weather phenomena as illustrated in Fig. 4 repeatedly occurred on the nights of 5–11 August. The simulation for the period of 7–8 August was chosen for a detailed analysis. In the surface wind spatial distribution at 0100 UTC (1900 CST) (Fig. 4f), three bands of maximum wind speed can be noticed: a momentum front along the coast of the Gulf of Mexico [the elongated leading or advancing edge of the air mass with apparent gradient of wind speed across the edge, as well as gradients of other characteristics (e.g., temperature, and moisture)] and two wind maximum bands (one near DFW along the Balcones Fault and the other to the west of DFW).

1) UPSLOPE WINDS ALONG THE SLOPING TERRAINS

The two wind maximum bands are approximately along with the steepest terrain slope (Fig. 5b). These wind maximum bands developed in the afternoon (Fig. 5a), likely due to the thermal contrast between the elevated terrain west of the Balcones Fault and the adjacent low-lying ground east of the Balcones Fault. On summer afternoons, due to intense solar radiation, the elevated terrain acts as a heat source compared to its surroundings, and so the near-surface air temperature is normally higher than the air temperature above the adjacent low-lying ground (Fig. 4g). Upslope wind develops along the sloping terrains and a downward return flow develops simultaneously over the adjacent low-lying ground. Such thermally driven local circulation on a large scale is termed the mountain–plains solenoid (MPS) circulation (May and Wilczak 1993; Sun and Zhang 2012). In case moisture contrast (manifested as a dryline) is also present, such a local circulation is referred to as “dryline circulation.” The upward motion along the slopes and downward motion east of the slopes are confirmed in the simulated vertical velocity (Fig. 5c). The upslope winds are superimposed on the ambient winds, leading to the wind maximum bands. The downward motion associated with the local circulation suppressed the boundary layer development in the area east of DFW (Fig. 5d). During the nighttime, the upslope wind subsided and the two wind maximum bands became indiscernible in ~3 h. Such a diurnal cycle of the local circulation and its associated

upslope winds also explain the afternoon surface wind peaks, which were repeatedly observed around DFW (Fig. 3b). The detailed dynamics and diurnal cycle of MPS and dryline circulation as well as their impact on boundary layer meteorology were previously discussed (Sun and Ogura 1979; Sun and Wu 1992; Koch et al. 2001; Zaitchik et al. 2007; Wang and Xue 2012; Bao and Zhang 2013; Hu et al. 2014; Zhang et al. 2014), thus it is not the focus of this study.

2) SEA-BREEZE DEVELOPMENT AND INLAND PENETRATION

This study focuses on the momentum front along the coast of the Gulf of Mexico, which developed around noon in the presence of a strong thermal contrast between hot land and cool sea (Fig. 4e). The momentum front advanced inland all the way to DFW around midnight (Fig. 4k) and lost the front characteristics gradually afterward, becoming indistinguishable from the ambient continental atmosphere. An approximate timeline of the inland movement of the momentum front based on model outputs is illustrated in Fig. 6. Because of the enhanced horizontal momentum behind the front, near-surface vertical wind shear was enhanced, thus near-surface mechanical turbulence was elevated behind the front (see the enhanced vertical mixing in Figs. 4i and 4n as indicated by the enhanced eddy diffusivity). Behind the momentum front, the temperature appeared lower than that ahead of the front. However, a sharp contrast of temperature across the front like that in the wind speed cannot be identified (Figs. 4b,g,l). The contrast of relative humidity (RH) behind and ahead of the front appeared sharper than that of temperature (Figs. 4c,h,m). Behind the front, RH was clearly higher than that ahead of the front. The movement direction and the contrasts of all the variables across the front suggested a typical marine air mass behind the front, which is cooler and moister than the continental air mass ahead of the front. Such an inland movement of cool and moist marine air in the form of a front appeared similar to inland penetration of sea breezes. However, the extent of inland penetration of sea breeze (or the horizontal scale of the sea-breeze circulation cell) in midlatitude regions (above $\sim 30^\circ$ latitude) is normally less than 200 km (Finkele et al. 1995; Miller et al. 2003; Crosman and Horel 2010), which is much less than the inland movement of the front in this case (~ 400 km from the coast to DFW). Thus, the inland movement of the front was not due to the growth of sea-breeze circulation cell, but appeared to be due to the advection of sea-breeze front by the environmental flow.

During the early evening transition, due to radiation cooling, the thermal contrast between the elevated terrain and plains cannot continue to provide the driving

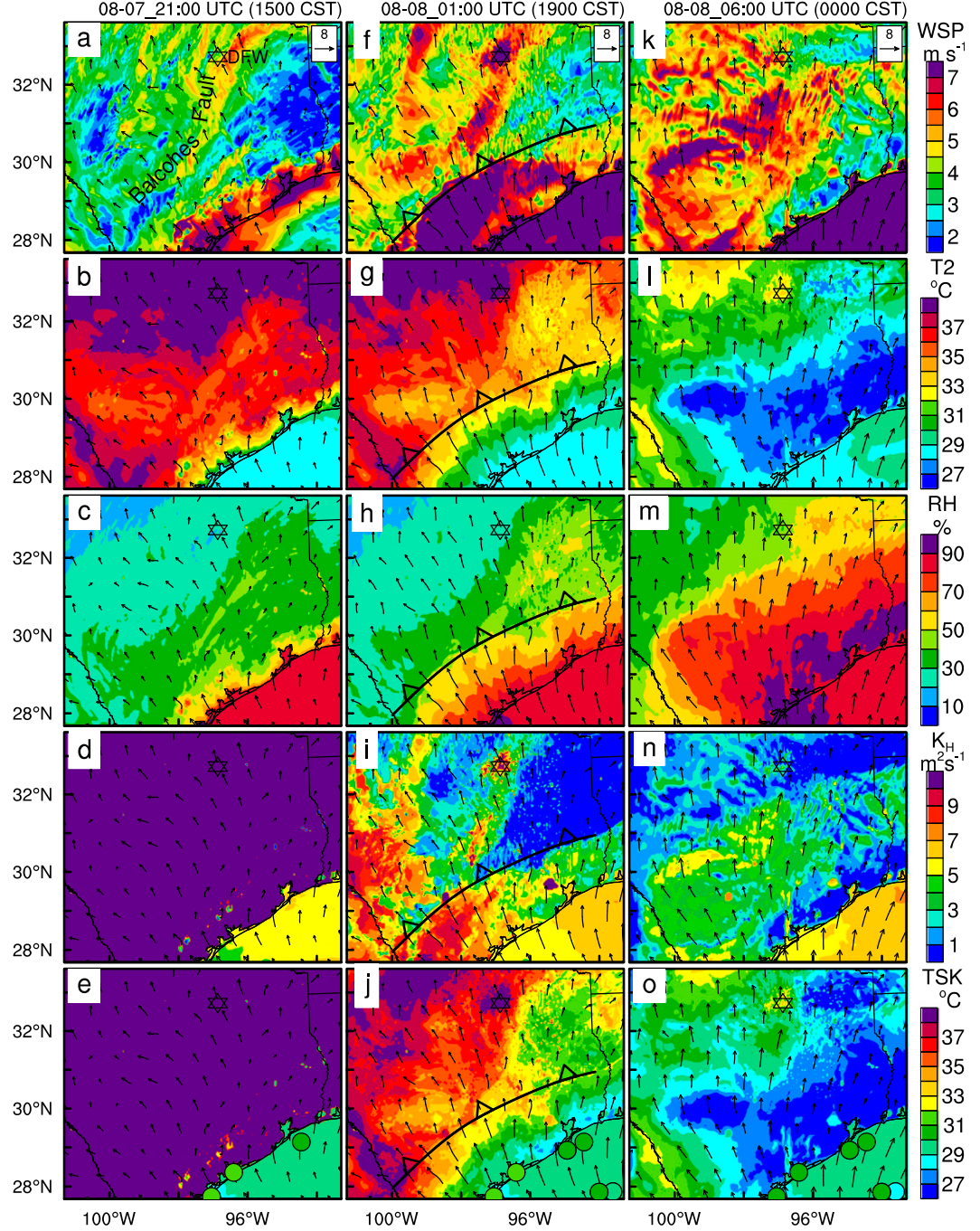


FIG. 4. Spatial distribution of simulated (a),(f),(k) 10-m wind speed (WSP); (b),(g),(l) 2-m temperature (T2); (c),(h),(m) 2-m relative humidity (RH); (d),(i),(n) near-surface eddy diffusivity (K_H); and (e),(j),(o) skin temperature (TSK) at (left to right) 2100 UTC (1500 CST), 0100 UTC (1900 CST), and 0600 UTC (0000 CST) on 7–8 Aug 2011. Note TSK over the ocean is equivalent to SST. The observed SST archived in the MADIS maritime data are indicated by shaded circles in (e),(j),(o). The sea-breeze front location at 0100 UTC is marked with weather front lines. The location of DFW is marked with stars.

force for the upslope winds, thus the wind band associated with the mountain–plain flow is advected northward by the prevailing environmental flow, just like the sea-breeze circulation. So the northward advection of

the wind band and the sea-breeze momentum front do not affect each other. The energy of the mountain–plain flow appears to be weaker than the sea-breeze circulation, thus the wind band associated with the mountain–plain flow

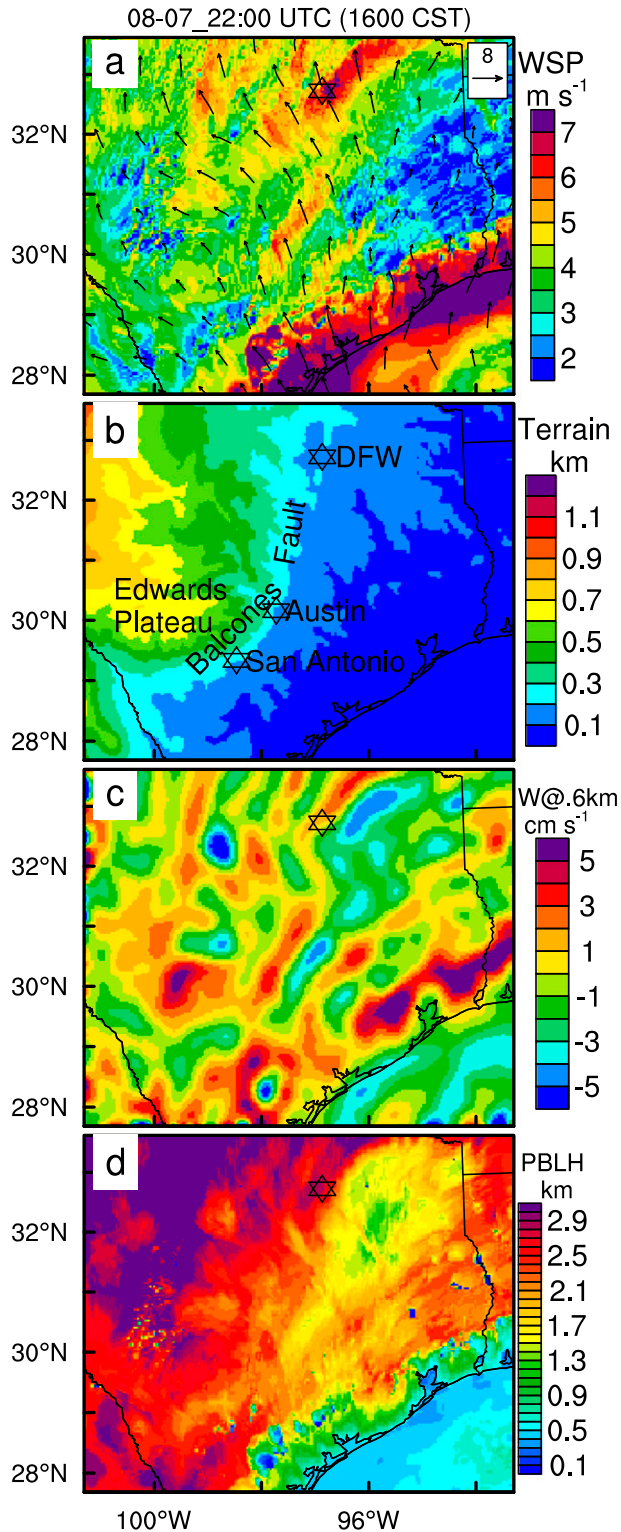


FIG. 5. Spatial distribution of (a) 10-m wind speed (WSP), (b) terrain height, (c) vertical velocity (W) at ~ 0.6 km AGL, and (d) boundary layer height (PBLH) at 2200 UTC (1600 CST) 7 Aug 2011.

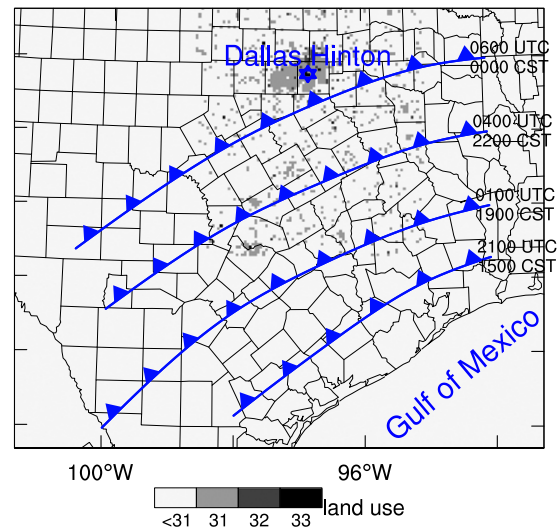


FIG. 6. Approximate locations of the momentum fronts identified from model simulated wind fields during the night of 7–8 Aug 2011. The corresponding time is marked.

merged into the background prevailing wind more quickly than the sea-breeze momentum front (figure not shown).

The inland movement of the sea-breeze front can be more clearly identified from the spatial distribution of tendencies (i.e., variation between the current and next hour). At the leading edge of the front, a belt of enhanced wind speed and RH was prominent during the course of the inland movement (Fig. 7). The leading edge of the front can also be identified from the enhanced eddy diffusivity induced by the enhanced wind shear (Figs. 7d,i). In the late evening the cooling band behind the front indicates the cool marine air mass behind the front. However, at the leading edge, cooling was not always found, instead, warming occurred at places (Fig. 7g). Such nocturnal warming was not prominent during the early evening transition (Fig. 7b) when the surface radiative cooling dominated. These belt shapes and their locations in the simulated tendencies were confirmed by the observed tendencies from the MADIS mesonet data. The inland movement of air mass with enhanced wind and RH in a belt shape parallel to the Gulf (Fig. 8) resembled the simulation (Fig. 7). The momentum front approached DFW around midnight (Figs. 7f and 8d), which explained the nocturnal wind maxima that manifested in the time series of wind speeds at the CAMS sites around DFW (Fig. 3b). A warming belt in the late evening was also prominent in the spatial distribution of the observed temperature tendency (Fig. 8e) while such warming was not clear during the early evening (Fig. 8b). The agreement of the spatial distribution of near-surface meteorological variables between simulation and observations indicates

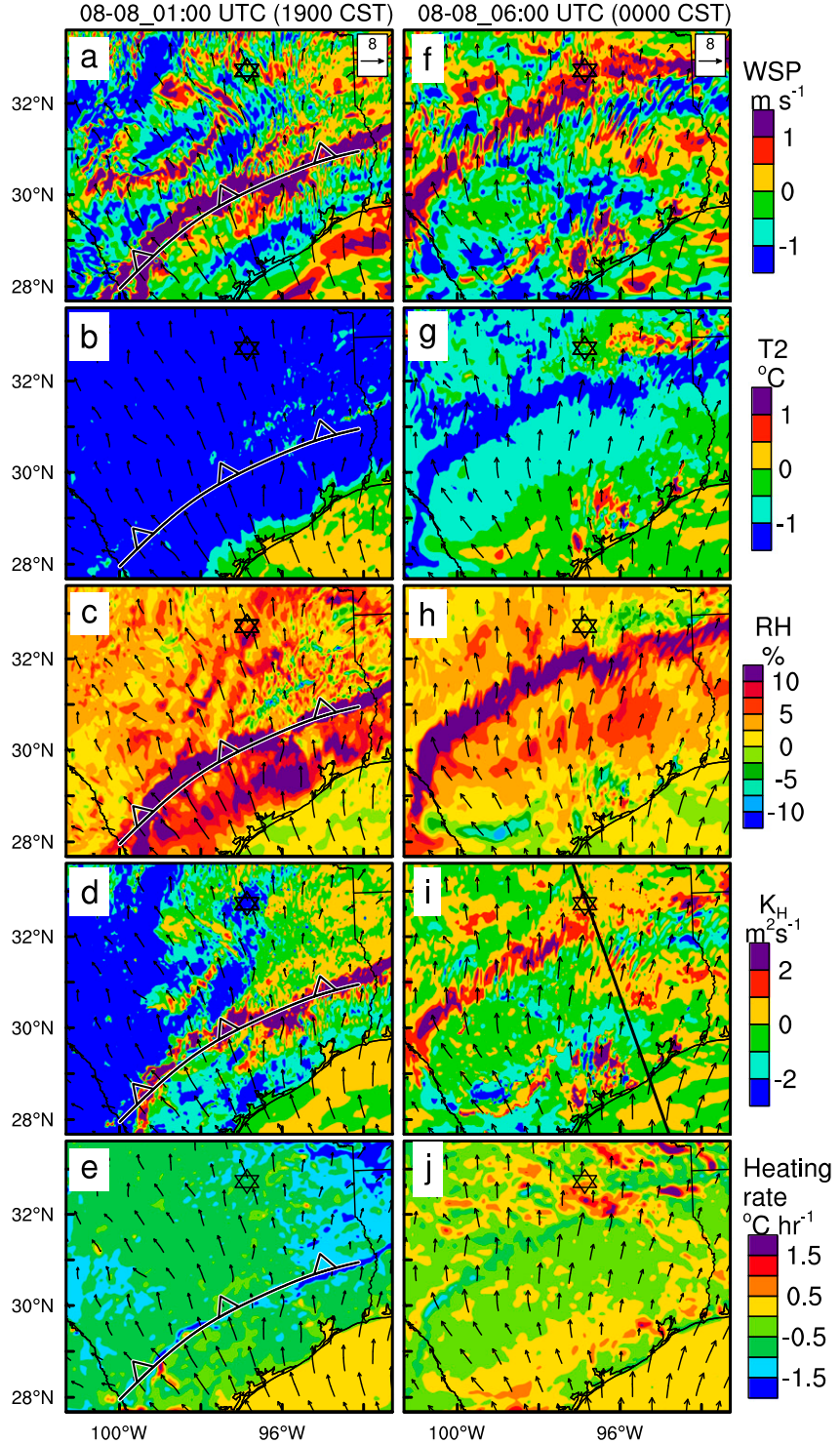


FIG. 7. Spatial distribution of simulated tendency (difference between next hour and current hour) of (a),(f) 10-m wind speed (WSP); (b),(g) 2-m temperature (T_2); (c),(h) 2-m relative humidity (RH); (d),(i) near-surface eddy diffusivity (K_H); and (e),(j) instantaneous heating rate of air in the first model layer due to vertical heat flux divergence at (left) 0100 UTC (1900 CST) and (right) 0600 UTC (0000 CST) 7–8 Aug 2011. The sea-breeze front location at 0100 UTC is marked with the weather front line. The location of DFW is marked with stars. The location of cross sections shown in Figs. 9, 11, and 12 is marked in (i).

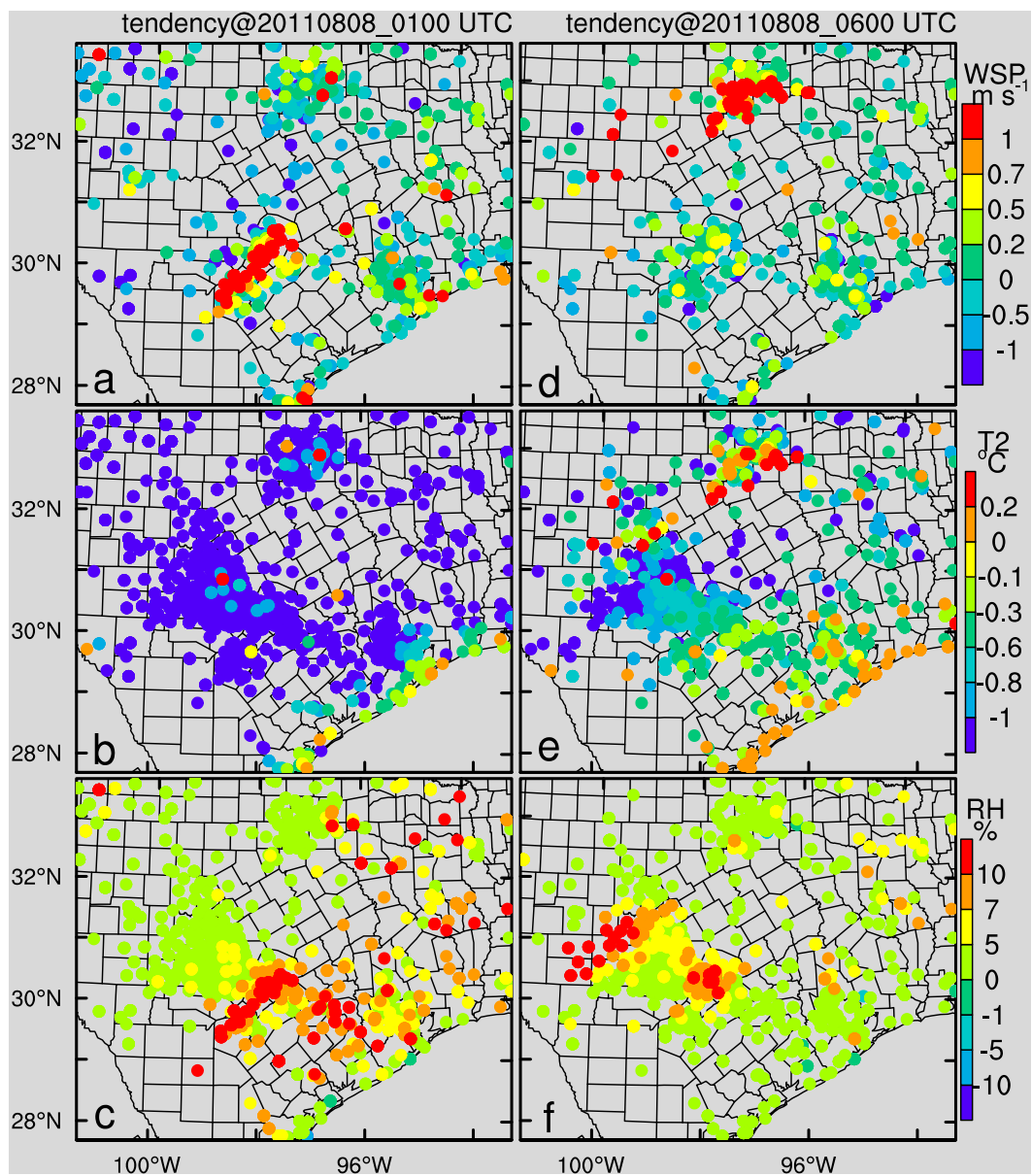


FIG. 8. Observed tendency of (a), (d) 10-m wind speed (WSP); (b), (e) 2-m temperature (T2); and (c), (f) 2-m relative humidity (RH) at MADIS mesonet sites at (left) 0100 UTC (1900 CST) and (right) 0600 UTC (0000 CST) on 7–8 Aug 2011.

that model bias in terms of the front propagation speed is small.

The impact of enhanced vertical mixing associated with the frontal passage on near-surface temperature is investigated using a budget analysis based on model outputs. Instantaneous heating rates of air in the first model layer due to vertical turbulent heat flux divergence are estimated (Figs. 7e,j). The vertical heat flux divergence is computed as the difference between the surface sensible heat flux (from the Noah land surface model) and the sensible heat flux at the interface of the

first and second model layers due to vertical turbulence mixing. Using a first-order closure approach, the latter can be calculated using the eddy diffusivity and the vertical temperature gradient. As shown in Fig. 7j, the heating rate at the leading edge of the front around midnight due to vertical turbulent heat flux divergence is close to the observed rural temperature increase rate ($\sim 0.5^{\circ}\text{C h}^{-1}$), which indicates that vertical turbulent mixing plays a dominant role in the rural nocturnal warming event. Note that in this budget analysis, neither the nonlocal turbulent flux nor the entrainment

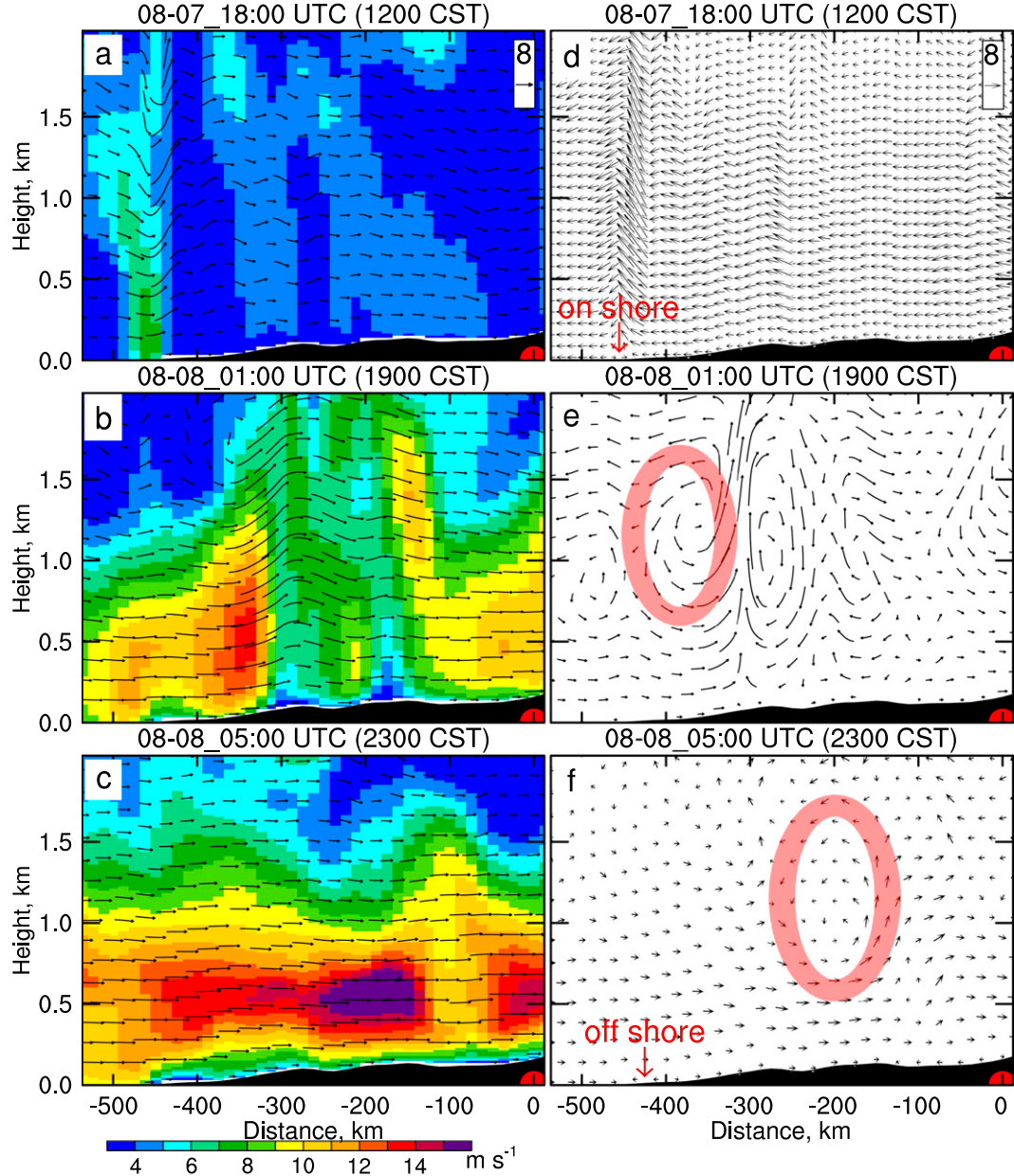


FIG. 9. Cross section of (a)–(c) wind and (d)–(f) its perturbation (difference from the mean) at (top to bottom) 1800 UTC (1200 CST), 0100 UTC (1900 CST), and 0500 UTC (2300 CST) 7–8 Aug 2011. The location of the cross section is marked in Fig. 7i. The color shading in (a)–(c) represent the horizontal wind speed. The sea-breeze circulation cells in the perturbation fields are marked in (e),(f). Note that vertical velocity is multiplied by 100 when plotting wind vectors. The position of DFW is marked by a red dot on the x axis.

flux is considered, which are considered in the YSU PBL scheme in the WRF Model.

c. Vertical structure of the sea-breeze front

The vertical structure of the front is illustrated in the cross section along a line perpendicular to the Gulf of Mexico (see the location of the cross section in Fig. 7i). A band with elevated horizontal wind (~ 40 km wide)

developed along the Gulf of Mexico around noontime (Fig. 9a), which indicate the feeder flow behind the sea-breeze front that persistently provides the air mass with marine characteristics during the day. The width of the band expanded to ~ 200 km wide around the early evening transition (Fig. 9b) and the band started to separate from the feeder flow and was advected by the prevailing southerly winds. During the

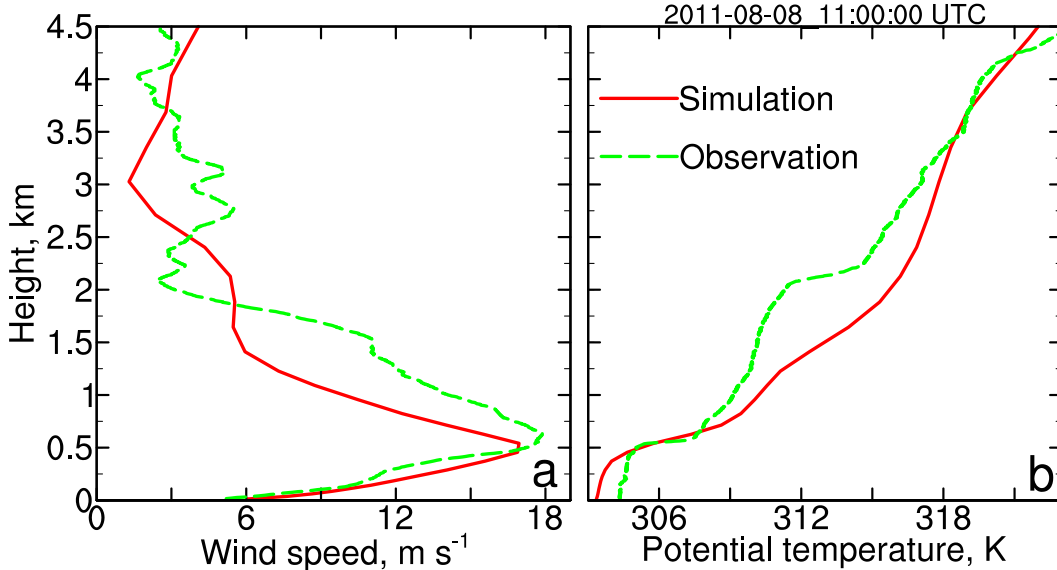


FIG. 10. Vertical profiles of (a) wind speed and (b) potential temperature at 1100 UTC (0500 CST) 11 Aug 2011 at Fort Worth (32.83508°N , 97.29794°W) simulated by the WRF Model and observed by the high vertical resolution radiosonde.

evening, a nocturnal low-level jet (LLJ) developed over the southern Great Plains, which further facilitates the advection of the wind band toward DFW (Fig. 9c). After passing DFW, the band with elevated wind gradually merged into the LLJs (figure not shown).

A closed sea-breeze circulation cell cannot be identified from the cross section of the instantaneous wind (Figs. 9a–c). Thus, a perturbation term is computed (i.e., the difference between the instantaneous wind and the mean wind during 7–8 August 2011). From the cross section of the wind perturbation, a closed sea-breeze circulation cell can be noticed to develop around noon (Fig. 9d) and it expanded to ~ 100 km wide until the early evening (Fig. 9e) and the closed circulation cell was advected along the LLJ (Fig. 9f). Thus, the cross section of the wind perturbation confirms the development of the sea-breeze front and its nighttime advection manifested in the horizontal spatial distributions (Figs. 4, 6, and 7). Since the prevailing wind was also onshore, the sea breeze in this case can be classified as the synoptic sea breeze, which is less studied in terms of its daytime development and nighttime movement comparing with other categories of sea breeze (Buckley and Kurzeja 1997; Miller et al. 2003; Crosman and Horel 2010; Steele et al. 2013). In the evening, due to the reversed thermal contrast between land and ocean, land breeze (offshore) developed near the surface along the coastal area in opposition to the prevailing southerly wind (Fig. 9f). Thus, a band of minimum wind appeared along the coast (Fig. 9c). This explains the separation of the sea-breeze

front from the coast during the nighttime inland movement seen in Figs. 4f and 4k.

The development of LLJ on the night of 7–8 August 2011 is confirmed by the vertical profiles observed at Fort Worth (achieved in HVRRD) (Fig. 10a). The strong inversion at ~ 500 m AGL effectively decouples the stable boundary layer from the residual layer above (Fig. 10b). Both observation and simulation demonstrate that the LLJ nose occurred at the top of the stable boundary layer, which can be explained by the Blackadar's inertial oscillation theory: the wind oscillation amplitude is expected to grow as the ground is approached from the top of the residual layer until the frictional force inevitably becomes important in the stable boundary layer (Shapiro and Fedorovich 2010), that is, the wind oscillation amplitude at night peaks at the top of the stable boundary layer. Because of the “Blackadar” mechanism and some other mechanisms, nocturnal LLJs occur frequently in the southern Great Plains in summer (Song et al. 2005; Hu et al. 2013c; Du and Rotunno 2014).

Because of the low-level convergence at the sea-breeze front, updrafts occurred along the front, creating the sea-breeze head. The updrafts brought moist marine air up to the top of the boundary layer (Fig. 11a), proving necessary impetus for cloud development. Figure 11b shows the resolved cloud water in the strong updrafts above the sea-breeze front. Note that the unresolved subgrid cumulus cloud cannot be derived from the model outputs. Thus, the model may underestimate total cloud water if subgrid-scale cumulus exists. The uncertainties associated with the microphysics scheme

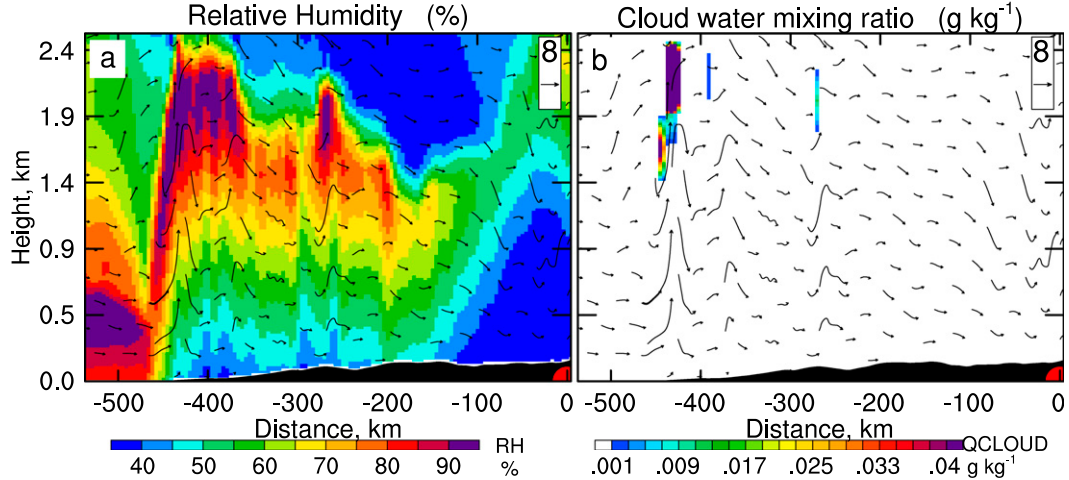


FIG. 11. Vertical cross section of simulated (a) relative humidity (RH) and (b) cloud water mixing ratio (QCLOUD) in domain 2 with a 4-km grid spacing at 1900 UTC (1200 CST) 7 Aug 2011. The position of DFW is marked by a red dot on the x axis.

may also affect the amount of simulated cumulus clouds (Fan et al. 2015). The vertically integrated resolved cloud water below 3 km (mostly cumulus) was simulated mostly over land along the Gulf of Mexico in the afternoon (figure not shown). The visible image from satellite confirms the scattered cumulus along the Gulf of Mexico (figure not shown). Such sea-breeze-associated updrafts and the subsequently induced cumulus clouds were often observed and simulated in coastal and adjacent inland areas (Helmis et al. 1987; Pielke et al. 1991; Chiba 1993; Simpson 1994; Atkins et al. 1995; Dias and Machado 1997; Stephan et al. 1999; Carbone et al. 2000; Rao and Fuelberg 2000; Shepherd et al. 2001).

Vertical cross sections of tendencies illustrate the inland movement of the sea-breeze front more clearly (Fig. 12). At 0100 UTC 8 August, the momentum front (leading edge of the maximum wind speed) moved ~ 160 km inland and the front moved farther (~ 340 km) inland at 0500 UTC. In the wind vector tendency, closed circulations were prominent (Figs. 12a,d). This further confirms the inland movement/advection of the sea-breeze circulation cell. Associated with the wind maximum bands, there are bands of elevated eddy diffusivity (Figs. 12b,e). This confirms the enhanced vertical mixing due to enhanced wind shear associated with the sea-breeze momentum front. Such enhanced turbulence induced by enhanced wind shear was also previously reported to occur during the passage of the sea-breeze fronts (Kitada 1987; Chiba 1993). The vertical cross sections of temperature tendency illustrate the inland movement of the thermodynamic front (defined as the interface of two air masses with the discontinuity of temperature). Following the leading edge of the

thermodynamic front, there are bands of decreased temperature, which indicate the inland movement of cool marine air (Figs. 12c,f). During the early evening, the thermodynamic front was straight upward (Fig. 12c) while the front inclined near midnight in the lower 300 m above the ground (Fig. 12f). Warming occurred near the surface around the momentum front around midnight (Fig. 12f), which corresponds to the near-surface warming belts seen in Figs. 7g and 8e; while such warming did not occur during the early evening (Figs. 12c, 7b, and 8b). During the early evening, due to surface cooling and diminished thermal turbulence (Wingo and Knupp 2015), in addition to advection of cool marine air, the cooling was straight up (as high as the sea-breeze head) at the leading edge of the sea-breeze momentum front. Ahead of the front, strong near-surface temperature inversion developed later into the evening in the ambient (continental) air due to continuous surface radiative cooling. During the passage of the sea-breeze momentum front, there was enhanced vertical mixing (Figs. 12b,e) in addition to the advection of cool marine air. Enhanced vertical mixing reduced the strong near-surface inversion and brought warmer air down to the surface around the momentum front. Such a warming process became dominant over other cooling processes late into the evening in the presence of strong temperature inversion, thus leading to the near-surface warming. As a consequent, the thermodynamic front inclined (Fig. 12f). Such a nocturnal warming mechanism is similar to that of the warming belts associated with synoptic-scale cold frontal passages (Doswell and Haugland 2007; Nallapareddy et al. 2011; Hu et al. 2013b). In both cases, enhanced vertical mixing associated with the momentum fronts played dominant

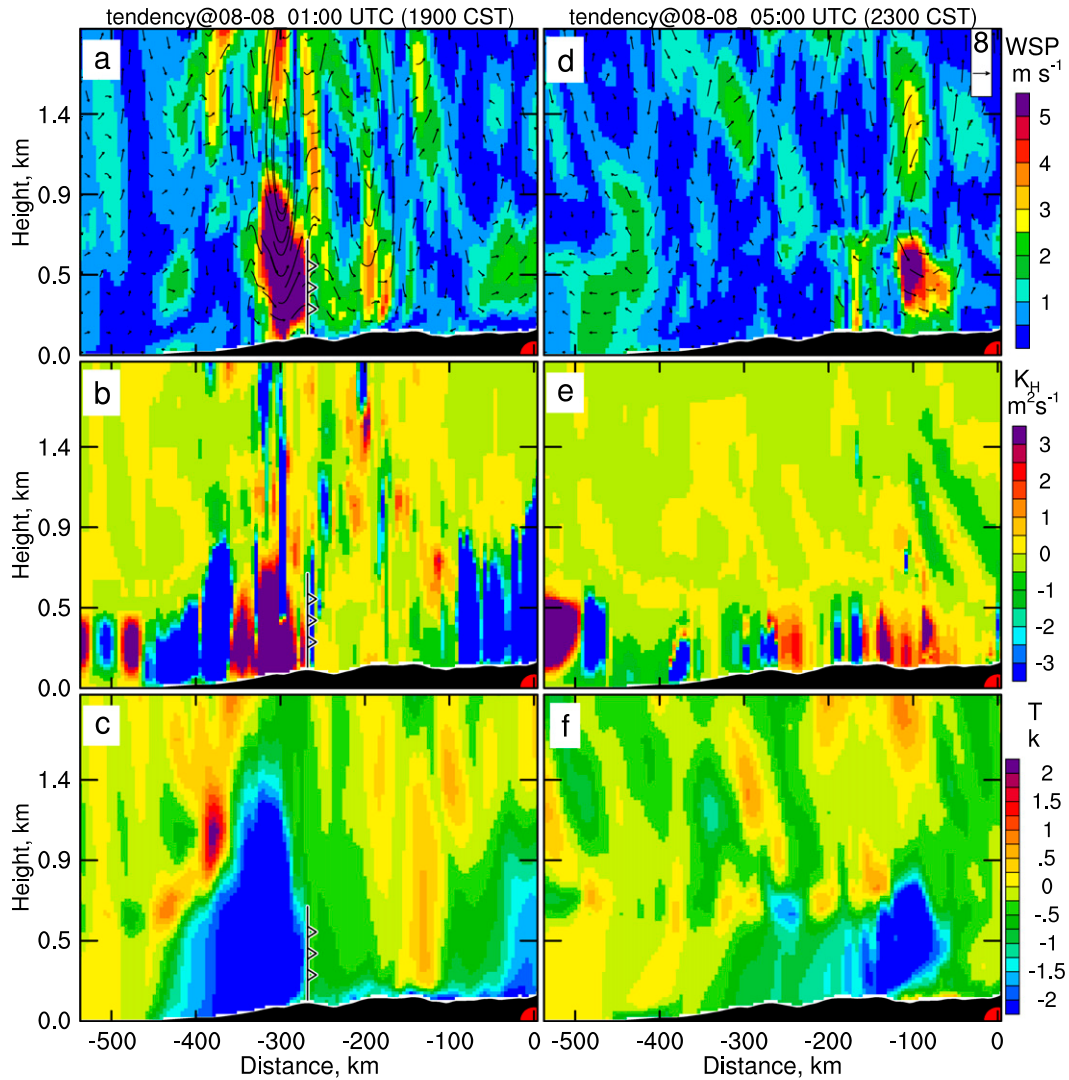


FIG. 12. Cross section of tendency of (a),(d) wind; (b),(e) eddy diffusivity (K_H); and (c),(f) temperature at (left) 0100 and (right) 0500 UTC 8 Aug 2011. The sea-breeze front location at 0100 UTC is marked with a weather front line.

roles. In places where strong near-surface temperature inversion did not develop before the frontal passage, surface warming did not occur (Figs. 7g and 8e).

d. Impact of the sea-breeze front on the UHI in DFW

In contrast to the rural continental air, where strong near-surface inversion develops in the evening due to surface radiative cooling, four major factors prevent a strong stable surface layer from developing in urban area: the release of heat stored in the urban materials during the day (Ogoli 2003; Liu et al. 2006; Zhu et al. 2009; Bohnenstengel et al. 2011; Yang et al. 2013), trapping of longwave radiation by urban buildings (Arnfield 2003), enhanced roughness (Hu et al. 2013c), and emission of anthropogenic heat (Ichinose et al. 1999;

Fan and Sailor 2005; Grossman-Clarke et al. 2005; Schlünzen et al. 2010). As a consequence, UHI developed around the metropolitan area of DFW (Fig. 13a) and it is successfully simulated by the WRF Model with SLUCM (Fig. 13b). A comparison of simulated skin temperatures (TSK) and land surface temperatures (LST) derived from the MODIS data is shown in Fig. 13. The model reproduces the MODIS-derived intensity and horizontal extent of the UHI well. A positive bias ($\sim 2^\circ\text{C}$) of WRF TSK comparing with MODIS LST can be noted, however, which may be due to model errors (Salamanca et al. 2011; Chen et al. 2012), the uncertainties in model inputs (e.g., insufficient soil moisture, Hu et al. 2010) and MODIS data (Wan and Li 2008). Similar differences between modeled TSK and MODIS LST in the southern

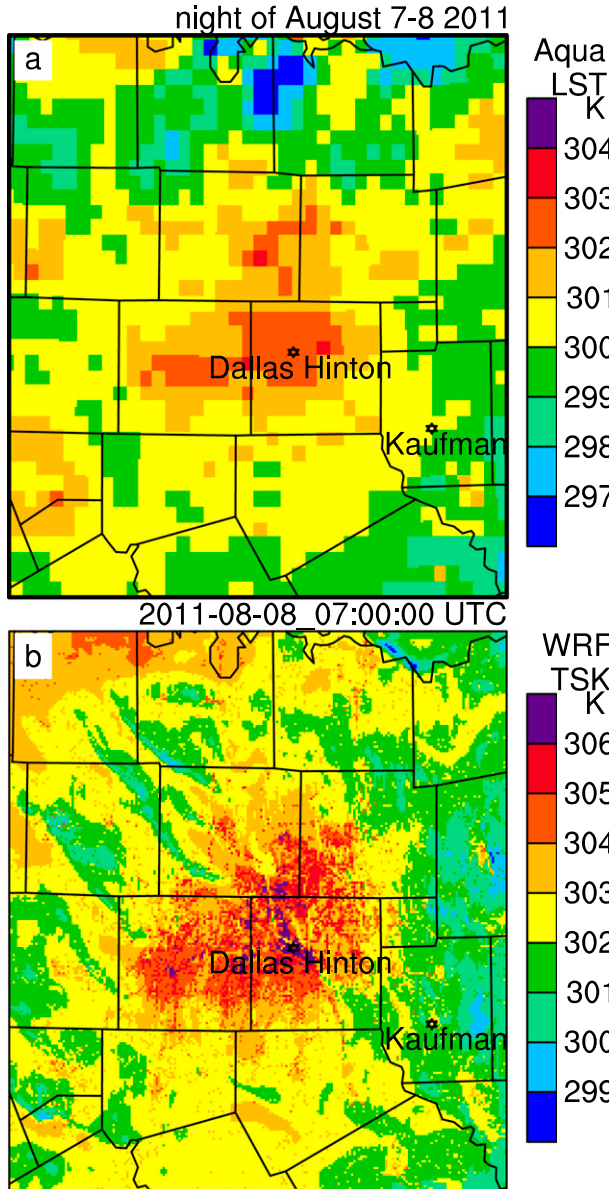


FIG. 13. Spatial distribution of (a) land surface temperatures (LST) retrieved from the *Aqua* MODIS data and (b) skin temperatures (TSK) simulated by WRF on 8 Aug 2011. The *Aqua* MODIS LST is at 0130 local time (nighttime overpass time), and the WRF TSK is at 0100 local time (0700 UTC).

Great Plains were also reported previously (Hu et al. 2013c). The relationship between the satellite-derived LST and air/skin temperature also needs further investigation to better interpret remotely sensed UHI (Roth et al. 1989; Arnfield 2003; Voogt and Oke 2003; Mohan et al. 2013).

UHI reduced the stability in the urban surface boundary layer. While a strong near-surface inversion developed in rural areas in relatively calm conditions

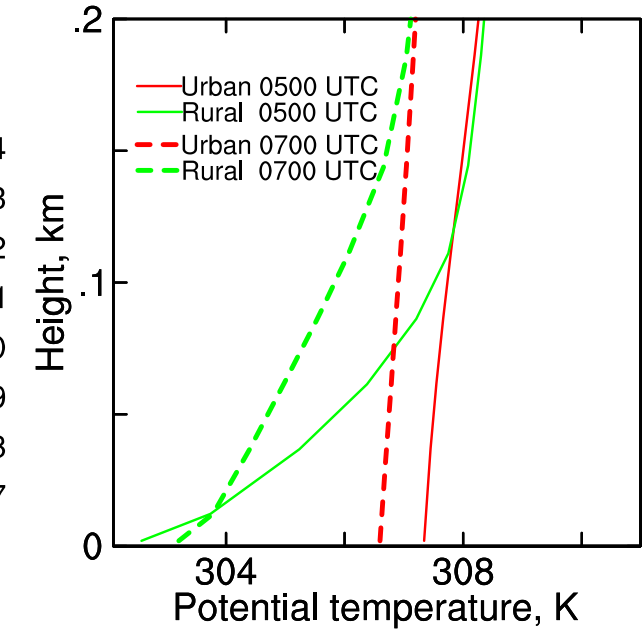


FIG. 14. WRF-simulated vertical profiles of potential temperature at urban (Dallas Hinton) and rural (Kaufman) areas before (0500 UTC) and after (0700 UTC) the frontal passage on 8 Aug 2011.

before the sea-breeze frontal passage, a nearly neutral boundary layer developed in urban areas (Fig. 14). A nearly neutral to even slightly unstable nocturnal boundary layer (could be up to ~ 200 m deep) is common over cities (Oke 1982; Rotach 1995; Lemonsu and Masson 2002; Martilli et al. 2002). After the sea-breeze frontal passage, the strong near-surface temperature inversion in rural areas was significantly reduced (Fig. 14) as a result of enhanced vertical mixing. The enhanced vertical mixing brought warmer air down to the surface. The warming process dominated over the cold advection and radiative cooling processes (Fig. 14), thus leading to the rural warming event near the surface (Figs. 14 and 15). Note that due to the different approaching time of the sea-breeze front, the nocturnal warming events occurred at the rural sites surrounding DFW at different times, but roughly around midnight. Such a warming mechanism explains the significant correlation between nocturnal wind maxima (indication of frontal passage) and the rural nocturnal warming events shown in Fig. 3. However, in urban area where the boundary layer was nearly neutral, enhanced mechanical vertical mixing associated with sea-breeze frontal passage did not alter the urban boundary layer significantly. The vertical temperature gradients in the urban boundary layer were barely changed (Fig. 14), suggesting that the warming process due to enhanced vertical mixing was negligible. Near-surface warming,

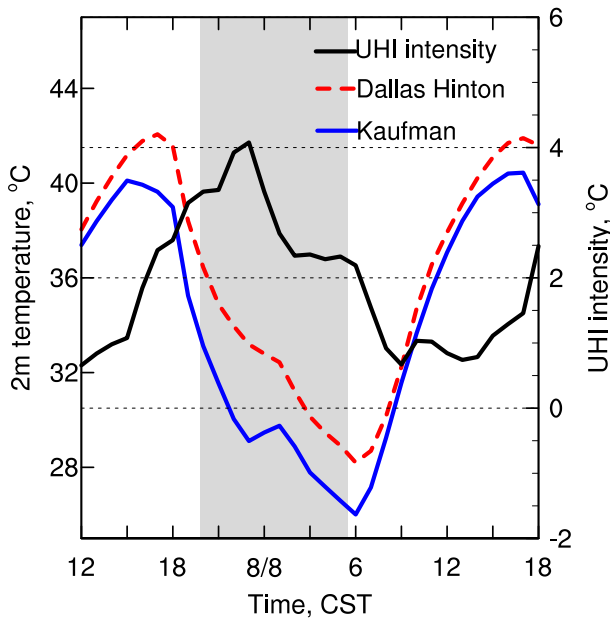


FIG. 15. Time series of temperature at Dallas Hinton and Kaufman and the resulting UHI intensity on 7–8 Aug 2011 simulated by the WRF Model. The period of sunset to sunrise is shaded.

therefore, did not occur in urban area (Figs. 3 and 15). As a result of nocturnal warming in rural area and no warming in urban area, reduction in the urban-rural temperature difference and, therefore, the collapse of UHI intensity around DFW occurred (Fig. 3). Even though certain bias can be noticed (e.g., near-surface temperature, which may be partially caused by model errors in the PBL scheme) (Hu et al. 2010, 2013a), the WRF Model with SLUCM successfully captured the sequence of relevant events, thus reproducing the collapse of the nocturnal UHI intensity (Fig. 15). These results can be summarized in another way: ahead of the front in a calm and very stable boundary layer the UHI is strong; during the sea-breeze front passage, enhanced wind shear and associated vertical mixing reduces the boundary layer stability, and the UHI is weakened. These results further highlight the importance of boundary layer stability on UHI assessments as previously pointed out in Hu et al. (2013c).

4. Conclusions and discussion

Investigation of UHI intensities of DFW (quantified as near-surface air temperature difference between representative urban and rural sites) in a heat wave episode revealed that “collapse” (sudden decrease) of nocturnal UHI intensities occurred frequently around midnight in August 2011. The UHI intensities in the later part of these nights were reduced to only half of the

intensities in the early part of the nights. Observational and modeling studies were conducted to understand such a unique temporal variation of the nocturnal UHI intensity. The surface meteorological data showed that the collapse of the nocturnal UHI intensity coincided with momentum front passages on those nights. The fronts developed along the Gulf of Mexico around noon and moved inland afterward and approached DFW (~400 km away from the Gulf Coast) around midnight. At the leading edge of the fronts, there was a band of increased wind speed and increased humidity. In the late evening, a warming belt was also noticed along the front edge while such warming was not prominent during the early evening.

WRF Model simulations were conducted to investigate the horizontal and vertical structures of the front. The inland movement of the belt with increased wind speed, increased humidity, and increased temperature was captured by the simulations. The vertical cross sections revealed that sea-breeze circulation cells (seen in the perturbation fields) developed along the Gulf Coast around noon due to the thermal contrast between warm land and cool ocean. The feeder flow behind the sea-breeze front persistently provides the air mass with marine characteristics during the day. The convergence at the sea-breeze front induced strong updrafts in the afternoon, which provided necessary impetus for cumulus cloud formation. Satellite visible images confirmed the belt of cumulus in the inland area along the Gulf of Mexico as induced by the sea-breeze updrafts. The sea-breeze circulation cells expanded to ~100 km wide until the early evening transition. Since the prevailing wind was onshore, the studied sea-breeze can be categorized as the synoptic sea breeze, a category that has received limited attention in the past in terms of its daytime development and nighttime movement.

After sunset, the thermal contrast reversed due to surface radiative cooling and a land breeze developed near the surface along the Gulf Coast. The remnant of daytime synoptic sea-breeze circulation cells were advected inland by the low-level jets and the front separated from the feeder flow. The advection of the cool and moist marine air in the form of fronts explains the inland movement of the belt with increased wind speed and increased humidity. Because of the enhanced wind shear associated with the sea-breeze momentum fronts, vertical mixing was enhanced at the leading edge of the fronts. Ahead of the fronts, surface radiative cooling increased near-surface temperature inversion through the night in a relatively calm condition. During the frontal passage (around midnight at DFW), the enhanced vertical mixing at the leading edge of the front decreased the strong temperature inversion and brought warmer air to the

surface, leading to rural surface warming. In contrast, urban effects prevented formation of a strong near-surface inversion in urban areas. The urban boundary layer was close to neutral. Thus, the enhanced mechanical mixing associated with the sea-breeze front could not alter the urban boundary layer significantly and thus did not cause surface warming in urban area. The different responses between rural (warming) and urban (no warming) areas to the sea-breeze frontal passages led to the collapse of the nocturnal UHI intensities in DFW.

A few environmental factors (e.g., diurnal cycle of differential heating, Coriolis force) control the horizontal scale of sea-breeze circulation and onshore penetration distance (Simpson et al. 1977; Rotunno 1983; Sha et al. 1991; Miller et al. 2003; Crosman and Horel 2010). The inland penetration of the sea breeze in the midlatitude region was reported to be within ~ 150 km (Miller et al. 2003; Crosman and Horel 2010). This study demonstrated that the sea-breeze circulation cells can be advected inland as far as 400 km while maintaining their characteristics (e.g., elevated wind speed, enhanced vertical mixing). Beyond 400 km, the circulation gradually merged with the ambient continental air. In addition, for the first time to our best knowledge, this study revealed that nocturnal warming events in rural areas (where strong near-surface inversion developed) can be induced by sea-breeze frontal passages. Similar nocturnal warming events were reported previously, but as results of a synoptic-scale cold front instead of sea-breeze front passages (Doswell and Haugland 2007; Nallapareddy et al. 2011; Hu et al. 2013b).

In addition to the UHIs, sea-breeze development also has important implications for air pollutants in coastal areas through transport/dispersion processes (Lyons and Olsson 1973; Physick and Abbs 1992; Gaza 1998; Clappier et al. 2000; Seaman and Michelson 2000; Gangoiti et al. 2002; Miller et al. 2003; Banta et al. 2005; Stuart et al. 2007; Yerramilli et al. 2008; Papanastasiou and Melas 2009; Papanastasiou et al. 2010). Most of these previous studies focused on daytime air quality issues (e.g., Banta et al. 2005) partially due to the belief that nighttime ozone (one of the key criteria pollutants) is not a concern because of its general low concentrations. However, recent studies (e.g., Banta et al. 1998; Reitebuch et al. 2000; Salmond and McKendry 2002; Talbot et al. 2005; Hu et al. 2012; Hu et al. 2013d; Kulkarni et al. 2013; Klein et al. 2014) suggested that nighttime secondary ozone maxima may occur as results of vertical mixing processes, which may be significant enough to become a concern to public health. Though not shown here, air quality data from the TCEQ CAMS sites were also examined. In addition to inducing rural

nocturnal warming events, the enhanced vertical mixing associated with the sea-breeze frontal passages also impacted boundary layer pollutants. Simultaneously as the collapse of the UHI intensity in DFW, nocturnal secondary ozone maxima often occurred near the surface in the DFW metropolitan area. These results will be reported elsewhere.

Acknowledgments. We are grateful to Tingting Qian for comments and suggestions. The second author was supported by NSF Grants AGS-0941491, AGS-1046171, AGS-1046081, and AGS-1261776. Computations were performed at the Texas Advanced Computing Center (TACC). Proofreading by David C. Doughty is greatly appreciated.

REFERENCES

- Abatan, A. A., B. J. Abiodun, and B. J. Omotosho, 2014: On the characteristics of sea breezes over Nigerian coastal region. *Theor. Appl. Climatol.*, **116**, 93–102, doi:10.1007/s00704-013-0931-z.
- Allen, C. J. T., and R. Washington, 2014: The low-level jet dust emission mechanism in the central Sahara: Observations from Bordj-Badji Mokhtar during the June 2011 Fennec Intensive Observation Period. *J. Geophys. Res. Atmos.*, **119**, 2990–3015, doi:10.1002/2013JD020594.
- Arnfield, A. J., 2003: Two decades of urban climate research: A review of turbulence, exchanges of energy and water, and the urban heat island. *Int. J. Climatol.*, **23**, 1–26, doi:10.1002/joc.859.
- Arritt, R. W., 1993: Effects of the large-scale flow on characteristic features of the sea breeze. *J. Appl. Meteor.*, **32**, 116–125, doi:10.1175/1520-0450(1993)032<0116:EOTLSF>2.0.CO;2.
- Atkins, N. T., R. M. Wakimoto, and T. M. Weckwerth, 1995: Observations of the sea-breeze front during CaPE. Part II: Dual-Doppler and aircraft analysis. *Mon. Wea. Rev.*, **123**, 944–969, doi:10.1175/1520-0493(1995)123<0944:OOTSBF>2.0.CO;2.
- Banta, R. M., and Coauthors, 1998: Daytime buildup and nighttime transport of urban ozone in the boundary layer during a stagnation episode. *J. Geophys. Res.*, **103**, 22 519–22 544, doi:10.1029/98JD01020.
- , and Coauthors, 2005: A bad air day in Houston. *Bull. Amer. Meteor. Soc.*, **86**, 657–669, doi:10.1175/BAMS-86-5-657.
- Bao, X. H., and F. Q. Zhang, 2013: Impacts of the mountain-plains solenoid and cold pool dynamics on the diurnal variation of warm-season precipitation over northern China. *Atmos. Chem. Phys.*, **13**, 6965–6982, doi:10.5194/acp-13-6965-2013.
- Basara, J. B., P. K. Hall Jr., A. J. Schroeder, B. G. Illston, and K. L. Nemunaitis, 2008: Diurnal cycle of the Oklahoma City urban heat island. *J. Geophys. Res.*, **113**, D20109, doi:10.1029/2008JD010311.
- , H. G. Basara, B. G. Illston, and K. C. Crawford, 2010: The impact of the urban heat island during an intense heat wave in Oklahoma City. *Adv. Meteor.*, **2010**, 230365, doi:10.1155/2010/230365.
- Bohnenstengel, S. I., S. Evans, P. A. Clark, and S. E. Belcher, 2011: Simulations of the London urban heat island. *Quart. J. Roy. Meteor. Soc.*, **137**, 1625–1640, doi:10.1002/qj.855.
- Bougeault, P., and P. Lacarrere, 1989: Parameterization of orography-induced turbulence in a mesobeta-scale model. *Mon. Wea. Rev.*, **117**, 1872–1890, doi:10.1175/1520-0493(1989)117<1872:POOITI>2.0.CO;2.

- Buckley, R. L., and R. J. Kurzeja, 1997: An observational and numerical study of the nocturnal sea breeze. Part I: Structure and circulation. *J. Appl. Meteor.*, **36**, 1577–1598, doi:[10.1175/1520-0450\(1997\)036<1577:AOANSO>2.0.CO;2](https://doi.org/10.1175/1520-0450(1997)036<1577:AOANSO>2.0.CO;2).
- Camilloni, I., and M. Barrucand, 2012: Temporal variability of the Buenos Aires, Argentina, urban heat island. *Theor. Appl. Climatol.*, **107**, 47–58, doi:[10.1007/s00704-011-0459-z](https://doi.org/10.1007/s00704-011-0459-z).
- Carbone, R. E., J. W. Wilson, T. D. Keenan, and J. M. Hacker, 2000: Tropical island convection in the absence of significant topography. Part I: Life cycle of diurnally forced convection. *Mon. Wea. Rev.*, **128**, 3459–3480, doi:[10.1175/1520-0493\(2000\)128<3459:TICITA>2.0.CO;2](https://doi.org/10.1175/1520-0493(2000)128<3459:TICITA>2.0.CO;2).
- Changnon, S. A., K. E. Kunkel, and B. C. Reinke, 1996: Impacts and responses to the 1995 heat wave: A call to action. *Bull. Amer. Meteor. Soc.*, **77**, 1497–1506, doi:[10.1175/1520-0477\(1996\)077<1497:IARTTH>2.0.CO;2](https://doi.org/10.1175/1520-0477(1996)077<1497:IARTTH>2.0.CO;2).
- Chen, F., and J. Dudhia, 2001: Coupling an advanced land surface-hydrology model with the Penn State–NCAR MM5 modeling system. Part I: Model implementation and sensitivity. *Mon. Wea. Rev.*, **129**, 569–585, doi:[10.1175/1520-0493\(2001\)129<0569:CAALSH>2.0.CO;2](https://doi.org/10.1175/1520-0493(2001)129<0569:CAALSH>2.0.CO;2).
- , and Coauthors, 2012: Research priorities in observing and modeling urban weather and climate. *Bull. Amer. Meteor. Soc.*, **93**, 1725–1728, doi:[10.1175/BAMS-D-11-00217.1](https://doi.org/10.1175/BAMS-D-11-00217.1).
- , X. C. Yang, and W. P. Zhu, 2014: WRF simulations of urban heat island under hot-weather synoptic conditions: The case study of Hangzhou City, China. *Atmos. Res.*, **138**, 364–377, doi:[10.1016/j.atmosres.2013.12.005](https://doi.org/10.1016/j.atmosres.2013.12.005).
- Cheng, Y. Y., and D. W. Byun, 2008: Application of high resolution land use and land cover data for atmospheric modeling in the Houston–Galveston metropolitan area. Part I: Meteorological simulation results. *Atmos. Environ.*, **42**, 7795–7811, doi:[10.1016/j.atmosenv.2008.04.055](https://doi.org/10.1016/j.atmosenv.2008.04.055).
- Chiba, O., 1993: The turbulent characteristics in the lowest part of the sea-breeze front in the atmospheric surface-layer. *Bound.-Layer Meteor.*, **65**, 181–195, doi:[10.1007/BF00708823](https://doi.org/10.1007/BF00708823).
- Childs, P. P., and S. Raman, 2005: Observations and numerical simulations of urban heat island and sea breeze circulations over New York City. *Pure Appl. Geophys.*, **162**, 1955–1980, doi:[10.1007/s00024-005-2700-0](https://doi.org/10.1007/s00024-005-2700-0).
- Clappier, A., and Coauthors, 2000: Effect of sea breeze on air pollution in the Greater Athens area. Part I: Numerical simulations and field observations. *J. Appl. Meteor.*, **39**, 546–562, doi:[10.1175/1520-0450\(2000\)039<0546:EOSBOA>2.0.CO;2](https://doi.org/10.1175/1520-0450(2000)039<0546:EOSBOA>2.0.CO;2).
- Crosman, E. T., and J. D. Horel, 2010: Sea and lake breezes: A review of numerical studies. *Bound.-Layer Meteor.*, **137**, 1–29, doi:[10.1007/s10546-010-9517-9](https://doi.org/10.1007/s10546-010-9517-9).
- Cui, Y. Y., and B. de Foy, 2012: Seasonal variations of the urban heat island at the surface and the near-surface and reductions due to urban vegetation in Mexico City. *J. Appl. Meteor. Climatol.*, **51**, 855–868, doi:[10.1175/JAMC-D-11-0104.1](https://doi.org/10.1175/JAMC-D-11-0104.1).
- Dandou, A., M. Tombrou, and N. Soulakellis, 2009: The influence of the city of Athens on the evolution of the sea-breeze front. *Bound.-Layer Meteor.*, **131**, 35–51, doi:[10.1007/s10546-008-9306-x](https://doi.org/10.1007/s10546-008-9306-x).
- Davis, R. E., P. C. Knappenberger, P. J. Michaels, and W. M. Novicoff, 2003: Changing heat-related mortality in the United States. *Environ. Health Perspect.*, **111**, 1712–1718, doi:[10.1289/ehp.6336](https://doi.org/10.1289/ehp.6336).
- Doswell, C. A., and M. J. Haugland, 2007: A comparison of two cold fronts—Effects of the planetary boundary layer on the mesoscale. *Electron. J. Severe Storms Meteor.*, **2** (4). [Available online at <http://www.ejssm.org/ojs/index.php/ejssm/article/viewarticle/30/24>.]
- Dou, J., Y. Wang, R. Bornstein, and S. Miao, 2015: Observed spatial characteristics of Beijing urban climate impacts on summer thunderstorms. *J. Appl. Meteor. Climatol.*, **54**, 94–105, doi:[10.1175/JAMC-D-13-0355.1](https://doi.org/10.1175/JAMC-D-13-0355.1).
- Du, Y., and R. Rotunno, 2014: A simple analytical model of the nocturnal low-level jet over the Great Plains of the United States. *J. Atmos. Sci.*, **71**, 3674–3683, doi:[10.1175/JAS-D-14-0060.1](https://doi.org/10.1175/JAS-D-14-0060.1).
- Dudhia, J., 1989: Numerical study of convection observed during the Winter Monsoon Experiment using a mesoscale two-dimensional model. *J. Atmos. Sci.*, **46**, 3077–3107, doi:[10.1175/1520-0469\(1989\)046<3077:NSOCOD>2.0.CO;2](https://doi.org/10.1175/1520-0469(1989)046<3077:NSOCOD>2.0.CO;2).
- EPA, 2015: Access to monitored air quality data from EPA's Air Quality System (AQS) Data Mart. Accessed 2015. [Available online at <https://www.epa.gov/airdata>.]
- Fan, H. L., and D. J. Sailor, 2005: Modeling the impacts of anthropogenic heating on the urban climate of Philadelphia: A comparison of implementations in two PBL schemes. *Atmos. Environ.*, **39**, 73–84, doi:[10.1016/j.atmosenv.2004.09.031](https://doi.org/10.1016/j.atmosenv.2004.09.031).
- Fan, J. W., and Coauthors, 2015: Improving representation of convective transport for scale-aware parameterization: 1. Convection and cloud properties simulated with spectral bin and bulk microphysics. *J. Geophys. Res. Atmos.*, **120**, 3485–3509, doi:[10.1002/2014JD022142](https://doi.org/10.1002/2014JD022142).
- Fast, J. D., J. C. Torcolini, and R. Redman, 2005: Pseudovertical temperature profiles and the urban heat island measured by a temperature datalogger network in Phoenix, Arizona. *J. Appl. Meteor.*, **44**, 3–13, doi:[10.1175/JAM-2176.1](https://doi.org/10.1175/JAM-2176.1).
- Finkele, K., J. M. Hacker, H. Kraus, and R. A. D. Byron Scott, 1995: A complete sea-breeze circulation cell-derived from aircraft observations. *Bound.-Layer Meteor.*, **73**, 299–317, doi:[10.1007/BF00711261](https://doi.org/10.1007/BF00711261).
- Flagg, D. D., and P. A. Taylor, 2011: Sensitivity of mesoscale model urban boundary layer meteorology to the scale of urban representation. *Atmos. Chem. Phys.*, **11**, 2951–2972, doi:[10.5194/acp-11-2951-2011](https://doi.org/10.5194/acp-11-2951-2011).
- Freitas, E. D., C. M. Rozoff, W. R. Cotton, and P. L. S. Dias, 2007: Interactions of an urban heat island and sea-breeze circulations during winter over the metropolitan area of São Paulo, Brazil. *Bound.-Layer Meteor.*, **122**, 43–65, doi:[10.1007/s10546-006-9091-3](https://doi.org/10.1007/s10546-006-9091-3).
- Gangoiti, G., and Coauthors, 2002: Regional transport of pollutants over the Bay of Biscay: Analysis of an ozone episode under a blocking anticyclone in west-central Europe. *Atmos. Environ.*, **36**, 1349–1361, doi:[10.1016/S1352-2310\(01\)00536-2](https://doi.org/10.1016/S1352-2310(01)00536-2).
- Garratt, J. R., and W. L. Physick, 1985: The inland boundary-layer at low latitudes. 2. Sea-breeze influences. *Bound.-Layer Meteor.*, **33**, 209–231, doi:[10.1007/BF00052056](https://doi.org/10.1007/BF00052056).
- Gaza, R. S., 1998: Mesoscale meteorology and high ozone in the northeast United States. *J. Appl. Meteor.*, **37**, 961–977, doi:[10.1175/1520-0450\(1998\)037<961:MMHOI>2.0.CO;2](https://doi.org/10.1175/1520-0450(1998)037<961:MMHOI>2.0.CO;2).
- Giannaros, T. M., and D. Melas, 2012: Study of the urban heat island in a coastal Mediterranean City: The case study of Thessaloniki, Greece. *Atmos. Res.*, **118**, 103–120, doi:[10.1016/j.atmosres.2012.06.006](https://doi.org/10.1016/j.atmosres.2012.06.006).
- , —, I. A. Daglis, I. Keramitsoglou, and K. Kourtidis, 2013: Numerical study of the urban heat island over Athens (Greece) with the WRF model. *Atmos. Environ.*, **73**, 103–111, doi:[10.1016/j.atmosenv.2013.02.055](https://doi.org/10.1016/j.atmosenv.2013.02.055).
- Grossman-Clarke, S., J. A. Zehnder, W. L. Stefanov, Y. B. Liu, and M. A. Zoldak, 2005: Urban modifications in a mesoscale meteorological model and the effects on near-surface variables in an arid metropolitan region. *J. Appl. Meteor.*, **44**, 1281–1297, doi:[10.1175/JAM2286.1](https://doi.org/10.1175/JAM2286.1).

- Helmis, C. G., D. N. Asimakopoulos, D. G. Deligiorgi, and D. P. Lalas, 1987: Observations of sea-breeze fronts near the shoreline. *Bound.-Layer Meteor.*, **38**, 395–410, doi:[10.1007/BF00120854](https://doi.org/10.1007/BF00120854).
- Hong, S. Y., J. Dudhia, and S. H. Chen, 2004: A revised approach to ice microphysical processes for the bulk parameterization of clouds and precipitation. *Mon. Wea. Rev.*, **132**, 103–120, doi:[10.1175/1520-0493\(2004\)132<0103:ARATIM>2.0.CO;2](https://doi.org/10.1175/1520-0493(2004)132<0103:ARATIM>2.0.CO;2).
- , Y. Noh, and J. Dudhia, 2006: A new vertical diffusion package with an explicit treatment of entrainment processes. *Mon. Wea. Rev.*, **134**, 2318–2341, doi:[10.1175/MWR3199.1](https://doi.org/10.1175/MWR3199.1).
- Hsu, S. A., 1970: Coastal air-circulation system: Observations and empirical model. *Mon. Wea. Rev.*, **98**, 487–509, doi:[10.1175/1520-0493\(1970\)098<0487:CACSOA>2.3.CO;2](https://doi.org/10.1175/1520-0493(1970)098<0487:CACSOA>2.3.CO;2).
- , 1988: *Coastal Meteorology*. Academic Press, 260 pp.
- Hu, X. M., J. W. Nielsen-Gammon, and F. Q. Zhang, 2010: Evaluation of three planetary boundary layer schemes in the WRF Model. *J. Appl. Meteor. Climatol.*, **49**, 1831–1844, doi:[10.1175/2010JAMC2432.1](https://doi.org/10.1175/2010JAMC2432.1).
- , D. C. Doughty, K. J. Sanchez, E. Joseph, and J. D. Fuentes, 2012: Ozone variability in the atmospheric boundary layer in Maryland and its implications for vertical transport model. *Atmos. Environ.*, **46**, 354–364, doi:[10.1016/j.atmosenv.2011.09.054](https://doi.org/10.1016/j.atmosenv.2011.09.054).
- , P. M. Klein, and M. Xue, 2013a: Evaluation of the updated YSU planetary boundary layer scheme within WRF for wind resource and air quality assessments. *J. Geophys. Res. Atmos.*, **118**, 10 490–10 505, doi:[10.1002/jgrd.50823](https://doi.org/10.1002/jgrd.50823).
- , —, —, A. Shapiro, and A. Nallapareddy, 2013b: Enhanced vertical mixing associated with a nocturnal cold front passage and its impact on near-surface temperature and ozone concentration. *J. Geophys. Res. Atmos.*, **118**, 2714–2728, doi:[10.1002/jgrd.50309](https://doi.org/10.1002/jgrd.50309).
- , —, —, J. K. Lundquist, F. Q. Zhang, and Y. C. Qi, 2013c: Impact of low-level jets on the nocturnal urban heat island intensity in Oklahoma City. *J. Appl. Meteor. Climatol.*, **52**, 1779–1802, doi:[10.1175/JAMC-D-12-0256.1](https://doi.org/10.1175/JAMC-D-12-0256.1).
- , and Coauthors, 2013d: Impact of the vertical mixing induced by low-level jets on boundary layer ozone concentration. *Atmos. Environ.*, **70**, 123–130, doi:[10.1016/j.atmosenv.2012.12.046](https://doi.org/10.1016/j.atmosenv.2012.12.046).
- , and Coauthors, 2014: Impact of the Loess Plateau on the atmospheric boundary layer structure and air quality in the North China Plain: A case study. *Sci. Total Environ.*, **499**, 228–237, doi:[10.1016/j.scitotenv.2014.08.053](https://doi.org/10.1016/j.scitotenv.2014.08.053).
- Ichinose, T., K. Shimodzono, and K. Hanaki, 1999: Impact of anthropogenic heat on urban climate in Tokyo. *Atmos. Environ.*, **33**, 3897–3909, doi:[10.1016/S1352-2310\(99\)00132-6](https://doi.org/10.1016/S1352-2310(99)00132-6).
- IPCC, 2007: *Climate Change 2007: The Physical Science Basis*. Cambridge University Press, 996 pp.
- Janjić, Z. I., 1990: The step-mountain coordinate—Physical package. *Mon. Wea. Rev.*, **118**, 1429–1443, doi:[10.1175/1520-0493\(1990\)118<1429:TSMCPP>2.0.CO;2](https://doi.org/10.1175/1520-0493(1990)118<1429:TSMCPP>2.0.CO;2).
- Keeler, J. M., and D. A. R. Kristovich, 2012: Observations of urban heat island influence on lake-breeze frontal movement. *J. Appl. Meteor. Climatol.*, **51**, 702–710, doi:[10.1175/JAMC-D-11-0166.1](https://doi.org/10.1175/JAMC-D-11-0166.1).
- Kim, Y., K. Sartelet, J. C. Raut, and P. Chazette, 2013: Evaluation of the Weather Research and Forecast/Urban Model over greater Paris. *Bound.-Layer Meteor.*, **149**, 105–132, doi:[10.1007/s10546-013-9838-6](https://doi.org/10.1007/s10546-013-9838-6).
- Kitada, T., 1987: Turbulence structure of sea breeze front and its implication in air pollution transport—Application of k- ϵ turbulence model. *Bound.-Layer Meteor.*, **41**, 217–239, doi:[10.1007/BF00120440](https://doi.org/10.1007/BF00120440).
- Klein, P., X.-M. Hu, and M. Xue, 2014: Impacts of mixing processes in nocturnal atmospheric boundary layer on urban ozone concentrations. *Bound.-Layer Meteor.*, **150**, 107–130, doi:[10.1007/s10546-013-9864-4](https://doi.org/10.1007/s10546-013-9864-4).
- Koch, S. E., F. Q. Zhang, M. L. Kaplan, Y. L. Lin, R. Weglarz, and C. M. Trexler, 2001: Numerical simulations of a gravity wave event over CCOPE. Part III: The role of a mountain-plains solenoid in the generation of the second wave episode. *Mon. Wea. Rev.*, **129**, 909–933, doi:[10.1175/1520-0493\(2001\)129<0909:NSOAGW>2.0.CO;2](https://doi.org/10.1175/1520-0493(2001)129<0909:NSOAGW>2.0.CO;2).
- Kulkarni, P. S., D. Bortoli, and A. M. Silva, 2013: Nocturnal surface ozone enhancement and trend over urban and suburban sites in Portugal. *Atmos. Environ.*, **71**, 251–259, doi:[10.1016/j.atmosenv.2013.01.051](https://doi.org/10.1016/j.atmosenv.2013.01.051).
- Kusaka, H., H. Kondo, Y. Kikegawa, and F. Kimura, 2001: A simple single-layer urban canopy model for atmospheric models: Comparison with multi-layer and slab models. *Bound.-Layer Meteor.*, **101**, 329–358, doi:[10.1023/A:1019207923078](https://doi.org/10.1023/A:1019207923078).
- Lee, T. W., J. Y. Lee, and Z.-H. Wang, 2012: Scaling of the urban heat island intensity using time-dependent energy balance. *Urban Climate*, **2**, 16–24, doi:[10.1016/j.uclim.2012.10.005](https://doi.org/10.1016/j.uclim.2012.10.005).
- Lemonsu, A., and V. Masson, 2002: Simulation of a summer urban breeze over Paris. *Bound.-Layer Meteor.*, **104**, 463–490, doi:[10.1023/A:1016509614936](https://doi.org/10.1023/A:1016509614936).
- , S. Belair, and J. Mailhot, 2009: The new Canadian urban modelling system: Evaluation for two cases from the Joint Urban 2003 Oklahoma City Experiment. *Bound.-Layer Meteor.*, **133**, 47–70, doi:[10.1007/s10546-009-9414-2](https://doi.org/10.1007/s10546-009-9414-2).
- Li, D., and E. Bou-Zeid, 2013: Synergistic interactions between urban heat islands and heat waves: The impact in cities is larger than the sum of its parts. *J. Appl. Meteor. Climatol.*, **52**, 2051–2064, doi:[10.1175/JAMC-D-13-02.1](https://doi.org/10.1175/JAMC-D-13-02.1).
- Li, M., Z. Mao, Y. Song, M. Liu, and X. Huang, 2015: Impacts of the decadal urbanization on thermally induced circulations in eastern China. *J. Appl. Meteor. Climatol.*, **54**, 259–282, doi:[10.1175/JAMC-D-14-0176.1](https://doi.org/10.1175/JAMC-D-14-0176.1).
- Li, X.-X., T.-Y. Koh, D. Entekhabi, M. Roth, J. Panda, and L. K. Norford, 2013: A multi-resolution ensemble study of a tropical urban environment and its interactions with the background regional atmosphere. *J. Geophys. Res. Atmos.*, **118**, 9804–9818, doi:[10.1002/jgrd.50795](https://doi.org/10.1002/jgrd.50795).
- Liu, Y. B., F. Chen, T. Warner, and J. Basara, 2006: Verification of a mesoscale data-assimilation and forecasting system for the Oklahoma City area during the Joint Urban 2003 field project. *J. Appl. Meteor. Climatol.*, **45**, 912–929, doi:[10.1175/JAM2383.1](https://doi.org/10.1175/JAM2383.1).
- Lyons, W. A., and L. E. Olsson, 1973: Detailed mesometeorological studies of air-pollution dispersion in Chicago lake breeze. *Mon. Wea. Rev.*, **101**, 387–403, doi:[10.1175/1520-0493\(1973\)101<0387:DMSOAP>2.3.CO;2](https://doi.org/10.1175/1520-0493(1973)101<0387:DMSOAP>2.3.CO;2).
- Martilli, A., A. Clappier, and M. W. Rotach, 2002: An urban surface exchange parameterisation for mesoscale models. *Bound.-Layer Meteor.*, **104**, 261–304, doi:[10.1023/A:1016099921195](https://doi.org/10.1023/A:1016099921195).
- May, P. T., and J. M. Wilczak, 1993: Diurnal and seasonal variations of boundary-layer structure observed with a radar wind profiler and RASS. *Mon. Wea. Rev.*, **121**, 673–682, doi:[10.1175/1520-0493\(1993\)121<0673:DASVOB>2.0.CO;2](https://doi.org/10.1175/1520-0493(1993)121<0673:DASVOB>2.0.CO;2).
- Memon, R. A., D. Y. C. Leung, and C. H. Liu, 2009: An investigation of urban heat island intensity (UHII) as an indicator of urban heating. *Atmos. Res.*, **94**, 491–500, doi:[10.1016/j.atmosres.2009.07.006](https://doi.org/10.1016/j.atmosres.2009.07.006).
- Miao, S. G., F. Chen, M. A. Lemone, M. Tewari, Q. C. Li, and Y. C. Wang, 2009: An observational and modeling study of characteristics of urban heat island and boundary layer structures in Beijing. *J. Appl. Meteor. Climatol.*, **48**, 484–501, doi:[10.1175/2008JAMC1909.1](https://doi.org/10.1175/2008JAMC1909.1).

- Miller, S. T. K., B. D. Keim, R. W. Talbot, and H. Mao, 2003: Sea breeze: Structure, forecasting, and impacts. *Rev. Geophys.*, **41**, 1011, doi:10.1029/2003RG000124.
- Mlawer, E. J., S. J. Taubman, P. D. Brown, M. J. Iacono, and S. A. Clough, 1997: Radiative transfer for inhomogeneous atmospheres: RRTM, a validated correlated-k model for the longwave. *J. Geophys. Res.*, **102**, 16 663–16 682, doi:10.1029/97JD00237.
- Mohan, M., Y. Kikegawa, B. R. Gurjar, S. Bhati, and N. R. Kolli, 2013: Assessment of urban heat island effect for different land use/land cover from micrometeorological measurements and remote sensing data for megacity Delhi. *Theor. Appl. Climatol.*, **112**, 647–658, doi:10.1007/s00704-012-0758-z.
- Morris, C. J. G., I. Simmonds, and N. Plummer, 2001: Quantification of the influences of wind and cloud on the nocturnal urban heat island of a large city. *J. Appl. Meteor.*, **40**, 169–182, doi:10.1175/1520-0450(2001)040<0169:QOTIOW>2.0.CO;2.
- Nallapareddy, A., A. Shapiro, and J. J. Gourley, 2011: A climatology of nocturnal warming events associated with cold-frontal passages in Oklahoma. *J. Appl. Meteor. Climatol.*, **50**, 2042–2061, doi:10.1175/JAMC-D-11-020.1.
- Nielsen-Gammon, J. W., 2012: The 2011 Texas drought: A briefing packet for the Texas Legislature October 31, 2011. OSC Rep., Texas A&M University, 44 pp. [Available online at http://climate.tamu.edu/files/2011_drought.pdf.]
- Ogoli, D. M., 2003: Predicting indoor temperatures in closed buildings with high thermal mass. *Energy Build.*, **35**, 851–862, doi:10.1016/S0378-7788(02)00246-3.
- Ohashi, Y., and H. Kida, 2002: Numerical experiments on the weak-wind region formed ahead of the sea-breeze front. *J. Meteor. Soc. Japan*, **80**, 519–527, doi:10.2151/jmsj.80.519.
- Oke, T. R., 1976: The distinction between canopy and boundary-layer urban heat islands. *Atmosphere*, **14**, 268–277.
- , 1981: Canyon geometry and the nocturnal urban heat-island—Comparison of scale model and field observations. *J. Climatol.*, **1**, 237, doi:10.1002/joc.3370010304.
- , 1982: The energetic basis of the urban heat island. *Quart. J. Roy. Meteor. Soc.*, **108**, 1–24, doi:10.1002/qj.49710845502.
- Papanastassiou, D. K., and D. Melas, 2009: Climatology and impact on air quality of sea breeze in an urban coastal environment. *Int. J. Climatol.*, **29**, 305–315, doi:10.1002/joc.1707.
- , —, T. Bartzanas, and C. Kittas, 2010: Temperature, comfort and pollution levels during heat waves and the role of sea breeze. *Int. J. Biometeor.*, **54**, 307–317, doi:10.1007/s00484-009-0281-9.
- Physick, W. L., and D. J. Abbs, 1992: Flow and plume dispersion in a coastal valley. *J. Appl. Meteor.*, **31**, 64–73, doi:10.1175/1520-0450(1992)031<0064:FAPDIA>2.0.CO;2.
- Pielke, R. A., A. Song, P. J. Michaels, W. A. Lyons, and R. W. Arritt, 1991: The predictability of sea-breeze generated thunderstorms. *Atmosfera*, **4**, 65–78.
- Pleim, J. E., 2007a: A combined local and nonlocal closure model for the atmospheric boundary layer. Part I: Model description and testing. *J. Appl. Meteor. Climatol.*, **46**, 1383–1395, doi:10.1175/JAM2539.1.
- , 2007b: A combined local and nonlocal closure model for the atmospheric boundary layer. Part II: Application and evaluation in a mesoscale meteorological model. *J. Appl. Meteor. Climatol.*, **46**, 1396–1409, doi:10.1175/JAM2534.1.
- Porson, A., D. G. Steyn, and G. Schayes, 2007: Formulation of an index for sea breezes in opposing winds. *J. Appl. Meteor. Climatol.*, **46**, 1257–1263, doi:10.1175/JAM2525.1.
- Qian, T. T., C. C. Epifanio, and F. Q. Zhang, 2012: Topographic effects on the tropical land and sea breeze. *J. Atmos. Sci.*, **69**, 130–149, doi:10.1175/JAS-D-11-011.1.
- Ramsey, N. R., P. M. Klein, and B. Moore, 2014: The impact of meteorological parameters on urban air quality. *Atmos. Environ.*, **86**, 58–67, doi:10.1016/j.atmosenv.2013.12.006.
- Rao, P. A., and H. E. Fuelberg, 2000: An investigation of convection behind the Cape Canaveral sea-breeze front. *Mon. Wea. Rev.*, **128**, 3437–3458, doi:10.1175/1520-0493(2000)128<3437:AIOCBT>2.0.CO;2.
- Reitebuch, O., A. Strassburger, S. Emeis, and W. Kuttler, 2000: Nocturnal secondary ozone concentration maxima analysed by sodar observations and surface measurements. *Atmos. Environ.*, **34**, 4315–4329, doi:10.1016/S1352-2310(00)00185-0.
- Rotach, M. W., 1995: Profiles of turbulence statistics in and above an urban street canyon. *Atmos. Environ.*, **29**, 1473–1486, doi:10.1016/1352-2310(95)00084-C.
- Roth, M., T. R. Oke, and W. J. Emery, 1989: Satellite-derived urban heat islands from three coastal cities and the utilization of such data in urban climatology. *Int. J. Remote Sens.*, **10**, 1699–1720, doi:10.1080/01431168908904002.
- Rotunno, R., 1983: On the linear theory of the land and sea breeze. *J. Atmos. Sci.*, **40**, 1999–2009, doi:10.1175/1520-0469(1983)040<1999:OTLTOT>2.0.CO;2.
- Salamanca, F., A. Martilli, M. Tewari, and F. Chen, 2011: A study of the urban boundary layer using different urban parameterizations and high-resolution urban canopy parameters with WRF. *J. Appl. Meteor. Climatol.*, **50**, 1107–1128, doi:10.1175/2010jamc2538.1.
- Salmond, J. A., and I. G. McKendry, 2002: Secondary ozone maxima in a very stable nocturnal boundary layer: Observations from the Lower Fraser Valley, BC. *Atmos. Environ.*, **36**, 5771–5782, doi:10.1016/S1352-2310(02)00698-2.
- Sarkar, A., R. S. Saraswat, and A. Chandrasekar, 1998: Numerical study of the effects of urban heat island on the characteristic features of the sea breeze circulation. *Proc. Ind. Acad. Sci.-Earth Planet. Sci.*, **107**, 127–137, doi:10.1007/BF02840463.
- Schlünzen, K. H., P. Hoffmann, G. Rosenhagen, and W. Riecke, 2010: Long-term changes and regional differences in temperature and precipitation in the metropolitan area of Hamburg. *Int. J. Climatol.*, **30**, 1121–1136, doi:10.1002/joc.1968.
- Seaman, N. L., and S. A. Michelson, 2000: Mesoscale meteorological structure of a high-ozone episode during the 1995 NARSTO-Northeast study. *J. Appl. Meteor.*, **39**, 384–398, doi:10.1175/1520-0450(2000)039<0384:MMSOAH>2.0.CO;2.
- Sha, W., T. Kawamura, and H. Ueda, 1991: A numerical study on sea/land breezes as a gravity current: Kelvin-Helmholtz billows and inland penetration of the sea-breeze front. *J. Atmos. Sci.*, **48**, 1649–1665, doi:10.1175/1520-0469(1991)048<1649:ANSOSB>2.0.CO;2.
- Shapiro, A., and E. Fedorovich, 2010: Analytical description of a nocturnal low-level jet. *Quart. J. Roy. Meteor. Soc.*, **136**, 1255–1262, doi:10.1002/qj.628.
- , P. M. Klein, S. C. Arms, D. Bodine, and M. Carney, 2009: The Lake Thunderbird Micronet Project. *Bull. Amer. Meteor. Soc.*, **90**, 811–823, doi:10.1175/2008BAMS2727.1.
- Shepherd, J. M., B. S. Ferrier, and P. S. Ray, 2001: Rainfall morphology in Florida convergence zones: A numerical study. *Mon. Wea. Rev.*, **129**, 177–197, doi:10.1175/1520-0493(2001)129<0177:RMIFCZ>2.0.CO;2.
- Silva Dias, M. A. F., and A. J. Machado, 1997: The role of local circulations in summertime convective development and nocturnal fog in São Paulo, Brazil. *Bound.-Layer Meteor.*, **82**, 135–157, doi:10.1023/A:1000241602661.
- Simpson, J. E., 1994: *Sea Breeze and Local Winds*. Cambridge University Press, 234 pp.

- , D. A. Mansfield, and J. R. Milford, 1977: Inland penetration of sea-breeze fronts. *Quart. J. Roy. Meteor. Soc.*, **103**, 47–76, doi:[10.1002/qj.49710343504](https://doi.org/10.1002/qj.49710343504).
- Skamarock, W. C., and Coauthors, 2008: A description of the Advanced Research WRF version 3. NCAR Tech. Note TN-475+STR, 113 pp., doi:[10.5065/D68S4MVH](https://doi.org/10.5065/D68S4MVH).
- Smoliak, B. V., P. K. Snyder, T. E. Twine, P. M. Mykleby, and W. F. Hertel, 2015: Dense network observations of the Twin Cities canopy-layer urban heat island. *J. Appl. Meteor. Climatol.*, **54**, 1899–1917, doi:[10.1175/JAMC-D-14-0239.1](https://doi.org/10.1175/JAMC-D-14-0239.1).
- Song, J., K. Liao, R. L. Coulter, and B. M. Lesht, 2005: Climatology of the low-level jet at the southern Great Plains atmospheric Boundary Layer Experiments site. *J. Appl. Meteor.*, **44**, 1593–1606, doi:[10.1175/JAM2294.1](https://doi.org/10.1175/JAM2294.1).
- Souch, C., and S. Grimmond, 2006: Applied climatology: Urban climate. *Prog. Phys. Geogr.*, **30**, 270–279, doi:[10.1191/030913306pp484pr](https://doi.org/10.1191/030913306pp484pr).
- Steele, C. J., S. R. Dorling, R. von Glasow, and J. Bacon, 2013: Idealized WRF model sensitivity simulations of sea breeze types and their effects on offshore windfields. *Atmos. Chem. Phys.*, **13**, 443–461, doi:[10.5194/acp-13-443-2013](https://doi.org/10.5194/acp-13-443-2013).
- , —, R. von Glasow, and J. Bacon, 2015: Modelling sea-breeze climatologies and interactions on coasts in the southern North Sea: Implications for offshore wind energy. *Quart. J. Roy. Meteor. Soc.*, **141**, 1821–1835, doi:[10.1002/qj.2484](https://doi.org/10.1002/qj.2484).
- Steeneneld, G. J., S. Koopmans, B. G. Heusinkveld, L. W. A. van Hove, and A. A. M. Holtslag, 2011: Quantifying urban heat island effects and human comfort for cities of variable size and urban morphology in the Netherlands. *J. Geophys. Res.*, **116**, D20129, doi:[10.1029/2011JD015988](https://doi.org/10.1029/2011JD015988).
- Stephan, K., H. Kraus, C. M. Ewenz, and J. M. Hacker, 1999: Sea-breeze front variations in space and time. *Meteor. Atmos. Phys.*, **70**, 81–95, doi:[10.1007/s007030050026](https://doi.org/10.1007/s007030050026).
- Stuart, A. L., A. Aksoy, F. Q. Zhang, and J. W. Nielsen-Gammon, 2007: Ensemble-based data assimilation and targeted observation of a chemical tracer in a sea breeze model. *Atmos. Environ.*, **41**, 3082–3094, doi:[10.1016/j.atmosenv.2006.11.046](https://doi.org/10.1016/j.atmosenv.2006.11.046).
- Sun, J. H., and F. Q. Zhang, 2012: Impacts of mountain-plains solenoid on diurnal variations of rainfalls along the mei-yu front over the east China plains. *Mon. Wea. Rev.*, **140**, 379–397, doi:[10.1175/MWR-D-11-00041.1](https://doi.org/10.1175/MWR-D-11-00041.1).
- Sun, W. Y., and Y. Ogura, 1979: Boundary-layer forcing as a possible trigger to a squall-line formation. *J. Atmos. Sci.*, **36**, 235–254, doi:[10.1175/1520-0469\(1979\)036<0235:BLFAAP>2.0.CO;2](https://doi.org/10.1175/1520-0469(1979)036<0235:BLFAAP>2.0.CO;2).
- , and C. C. Wu, 1992: Formation and diurnal variation of the dryline. *J. Atmos. Sci.*, **49**, 1606–1619, doi:[10.1175/1520-0469\(1992\)049<1606:FADVOT>2.0.CO;2](https://doi.org/10.1175/1520-0469(1992)049<1606:FADVOT>2.0.CO;2).
- Tadesse, T., B. D. Wardlow, J. F. Brown, M. D. Svoboda, M. J. Hayes, B. Fuchs, and D. Gutzmer, 2015: Assessing the vegetation condition impacts of the 2011 drought across the U.S. Southern Great Plains using the Vegetation Drought Response Index (VegDRI). *J. Appl. Meteor. Climatol.*, **54**, 153–169, doi:[10.1175/JAMC-D-14-0048.1](https://doi.org/10.1175/JAMC-D-14-0048.1).
- Talbot, R., H. T. Mao, and B. Sive, 2005: Diurnal characteristics of surface level O₃ and other important trace gases in New England. *J. Geophys. Res.*, **110**, D09307, doi:[10.1029/2004JD005449](https://doi.org/10.1029/2004JD005449).
- Tan, J. G., and Coauthors, 2010: The urban heat island and its impact on heat waves and human health in Shanghai. *Int. J. Biometeor.*, **54**, 75–84, doi:[10.1007/s00484-009-0256-x](https://doi.org/10.1007/s00484-009-0256-x).
- Theeuwes, N. E., A. Solcerova, and G. J. Steeneveld, 2013: Modeling the influence of open water surfaces on the summertime temperature and thermal comfort in the city. *J. Geophys. Res. Atmos.*, **118**, 8881–8896, doi:[10.1002/jgrd.50704](https://doi.org/10.1002/jgrd.50704).
- Thompson, W. T., T. Holt, and J. Pullen, 2007: Investigation of a sea breeze front in an urban environments. *Quart. J. Roy. Meteor. Soc.*, **133**, 579–594, doi:[10.1002/qj.52](https://doi.org/10.1002/qj.52).
- Tijm, A. B. C., A. A. M. Holtslag, and A. J. van Delden, 1999: Observations and modeling of the sea breeze with the return current. *Mon. Wea. Rev.*, **127**, 625–640, doi:[10.1175/1520-0493\(1999\)127<0625:OAMOTS>2.0.CO;2](https://doi.org/10.1175/1520-0493(1999)127<0625:OAMOTS>2.0.CO;2).
- Tumanov, S., A. Stan-Sion, A. Lupu, C. Soci, and C. Oprea, 1999: Influences of the city of Bucharest on weather and climate parameters. *Atmos. Environ.*, **33**, 4173–4183, doi:[10.1016/S1352-2310\(99\)00160-0](https://doi.org/10.1016/S1352-2310(99)00160-0).
- Unger, J., Z. Sumeghy, and J. Zoboki, 2001: Temperature cross-section features in an urban area. *Atmos. Res.*, **58**, 117–127, doi:[10.1016/S0169-8095\(01\)00087-4](https://doi.org/10.1016/S0169-8095(01)00087-4).
- Voogt, J. A., and T. R. Oke, 2003: Thermal remote sensing of urban climates. *Remote Sens. Environ.*, **86**, 370–384, doi:[10.1016/S0034-4257\(03\)00079-8](https://doi.org/10.1016/S0034-4257(03)00079-8).
- Wan, Z., and Z. L. Li, 2008: Radiance-based validation of the V5 MODIS land-surface temperature product. *Int. J. Remote Sens.*, **29**, 5373–5395, doi:[10.1080/01431160802036565](https://doi.org/10.1080/01431160802036565).
- Wang, Q.-W., and M. Xue, 2012: Convective initiation on 19 June 2002 during IHOP: High-resolution simulations and analysis of the mesoscale structures and convection initiation. *J. Geophys. Res.*, **117**, D12107, doi:[10.1029/2012JD017552](https://doi.org/10.1029/2012JD017552).
- White, L. D., 2009: Sudden nocturnal warming events in Mississippi. *J. Appl. Meteor. Climatol.*, **48**, 758–775, doi:[10.1175/2008JAMC1971.1](https://doi.org/10.1175/2008JAMC1971.1).
- Wingo, S., and K. Knupp, 2015: Multi-platform observations characterizing the afternoon-to-evening transition of the planetary boundary layer in northern Alabama, USA. *Boundary-Layer Meteor.*, **155**, 29–53, doi:[10.1007/s10546-014-9988-1](https://doi.org/10.1007/s10546-014-9988-1).
- Winguth, A. M. E., and B. Kelp, 2013: The urban heat island of the north-central Texas region and its relation to the 2011 severe Texas drought. *J. Appl. Meteor. Climatol.*, **52**, 2418–2433, doi:[10.1175/JAMC-D-12-0195.1](https://doi.org/10.1175/JAMC-D-12-0195.1).
- Yan, H., and R. A. Anthes, 1987: The effect of latitude on the sea breeze. *Mon. Wea. Rev.*, **115**, 936–956, doi:[10.1175/1520-0493\(1987\)115<0936:TEOLOT>2.0.CO;2](https://doi.org/10.1175/1520-0493(1987)115<0936:TEOLOT>2.0.CO;2).
- Yang, P., G. Y. Ren, and W. D. Liu, 2013: Spatial and temporal characteristics of Beijing urban heat island intensity. *J. Appl. Meteor. Climatol.*, **52**, 1803–1816, doi:[10.1175/JAMC-D-12-0125.1](https://doi.org/10.1175/JAMC-D-12-0125.1).
- Yerramilli, A., and Coauthors, 2008: Some observational and modeling studies of the atmospheric boundary layer at Mississippi Gulf Coast for air pollution dispersion assessment. *Int. J. Environ. Res. Public Health*, **5**, 484–497, doi:[10.3390/ijerph5050484](https://doi.org/10.3390/ijerph5050484).
- Zaitchik, B. F., J. P. Evans, and R. B. Smith, 2007: Regional impact of an elevated heat source: The Zagros Plateau of Iran. *J. Climate*, **20**, 4133–4146, doi:[10.1175/JCLI4248.1](https://doi.org/10.1175/JCLI4248.1).
- Zhang, Y. C., J. H. Sun, and S. M. Fu, 2014: Impacts of diurnal variation of mountain-plain solenoid circulations on precipitation and vortices east of the Tibetan Plateau during the mei-yu season. *Adv. Atmos. Sci.*, **31**, 139–153, doi:[10.1007/s00376-013-2052-0](https://doi.org/10.1007/s00376-013-2052-0).
- Zhu, L., R. Hurt, D. Correia, and R. Boehm, 2009: Detailed energy saving performance analyses on thermal mass walls demonstrated in a zero energy house. *Energy Build.*, **41**, 303–310, doi:[10.1016/j.enbuild.2008.10.003](https://doi.org/10.1016/j.enbuild.2008.10.003).